Shimada *et al.*
Progress in Earth and Planetary Science (2023) 10:49
https://doi.org/10.1186/s40645-023-00577-9

Progress in Earth and Planetary Science

RESEARCH ARTICLE

Open Access

Marine inundation history during the last 3000 years at Lake Kogare-ike, a coastal lake on the Pacific coast of central Japan

Yumi Shimada[1,2*], Yuki Sawai[1], Dan Matsumoto[1], Koichiro Tanigawa[1], Kazumi Ito[1], Toru Tamura[1,2], Yuichi Namegaya[1], Masanobu Shishikura[1] and Shigehiro Fujino[3]

Abstract

Sediment cores collected at Lake Kogare-ike, a coastal lake on the Pacific coast of central Japan, record the marine inundation history during the last 3000 years. The sediments consist mainly of organic mud, sand, gravel, inorganic mud, and volcanic ash, and inundation events were recognized as 19 event deposits (E1–E19, from top to bottom) interbedded with the organic mud. Visual observation by naked eyes and X-ray computed tomography (CT) images identified 16 event deposits based on quantitative and qualitative changes in sand contents and changes in the textures and colors of the sediment samples (E1–E3, E5, E6, E8, E9, and E11–E19). The other three event deposits (E4, E7, and E10) were identified only on the CT images as layers with higher radiodensity than the underlying and overlying organic mud layers. The sedimentary features, the spatial bias of the event deposits toward seaward areas, the diatom assemblages, and the frequency of inundation events suggest that 13 (E1–E10 and E12–E14) of the 19 event deposits were formed by tsunamis or extraordinary storms. To constrain the depositional ages of the event deposits, Bayesian age–depth models were constructed based on radiocarbon dating of plant macrofossils and concentrated fossil pollen and the ^{137}Cs profile. The depositional ages of the event deposits indicate that five or possibly six event deposits can be correlated with historical tsunamis along the Nankai Trough: E2, either of E3 or E4, E5, E7, and E9 correspond to the 1707 CE Hoei, the 1605 CE Keicho, the 1498 CE Meio, the 1096 CE Eicho, and the 684 CE Hakuho tsunamis, respectively. E1 was possibly formed by the 1944 CE Showa-Tonankai tsunami, the 1854 Ansei–Tokai tsunami, the 1959 Isewan typhoon, or a combination of two or all three events.

Keywords Bayesian age–depth model, Extreme events, Japan, Lacustrine sediments, Nankai trough, Storm surges, Tsunami

1 Introduction

Infrequent but extraordinary extreme waves, such as tsunamis and storms, impact coastal environments. Instrumental records (e.g., from tide gauges and oceanographic observation buoys) are generally available only for within the last century. Historical documents are also used to comprehend the history of past extreme wave events, but such events are difficult to reconstruct in detail on millennial or centennial timescales because of the shortness and/or incompleteness of historical records. To supplement these records and to extend the history of extreme events, geological records have been employed

*Correspondence:
Yumi Shimada
yumi.shimada@aist.go.jp
[1] Geological Survey of Japan, National Institute of Advanced Industrial Science and Technology (AIST), Higashi 1-1-1-C7, Tsukuba, Ibaraki 305-8567, Japan
[2] Graduate School of Frontier Sciences, The University of Tokyo, Kashiwanoha 5-1-5, Kashiwa, Chiba 277-8561, Japan
[3] Faculty of Life and Environmental Sciences, University of Tsukuba, Tennodai 1-1-1, Tsukuba, Ibaraki 305-8572, Japan

in tsunami geology (Hindson et al. 1996; Dawson et al. 1988, 2020; Atwater et al. 2005; Cisternas et al. 2005; Jankaew et al. 2008; Costa and Andrade 2020; Sawai 2020; Ishimura et al. 2022) and paleotempestology (Liu and Fearn 1993, 2000; Woodruff et al. 2009; Yao et al. 2020; Bianchette et al. 2022) worldwide to better understand the history of extreme waves and aid with prediction of future such events. In both research fields, event deposits within lacustrine and marshy sediments have served as a guide to reconstruct inundation areas (Nanayama et al. 2003; Sawai et al. 2012; Pilarczyk et al. 2021) and the recurrence history of extreme waves (Liu and Fearn 1993; Nanayama et al. 2003; Sawai et al. 2009a).

The Pacific coast of central and western Japan has been repeatedly inundated by tsunamis and storms (Arakawa et al. 1961; Watanabe 1998; Usami et al. 2013; Ishibashi 2014), but the inundation history over the past thousands of years has not been fully reconstructed. For tsunami history, the governmental long-term evaluation of subduction-zone earthquakes in this region is based mainly on historical documents recording the nine great earthquakes and their accompanying tsunamis that have occurred during the last 1300 years along the Nankai Trough (The Headquarters for Earthquake Research Promotion 2013; Fig. 1d). However, records of earthquakes before the seventeenth century are fewer and more fragmentary than those of earthquakes after the eighteenth century (Koyama 1999). Koyama (1999) pointed out that there is a lack of records for the medieval period or earlier. In addition, the 1300 years of history recorded in written documents is too short to evaluate earthquakes because unusually giant earthquakes recur at intervals of hundreds of years (Satake and Atwater 2007). In evaluations of storm surges and waves, the shortness of the historical and instrumental records is the most problematic issue. Written documents for the past 300 years show that the Pacific coastal areas of Japan have been repeatedly affected by storms (Arakawa et al. 1961), but there is little information on the exact values of inundation heights and distances. Specific data from instrumental records are available only for the past 70 years. Recent instrumental records have demonstrated that typhoons, as shown, for example, by the Isewan Typhoon in 1959, can cause widespread inundation of the Pacific coast of central Japan, but the frequency of such extraordinary typhoons is not known. Datasets based on geological records are therefore required for long-term assessment of coastal hazards resulting from marine inundation in this coastal area.

Geological evidence for tsunamis and storms has been reported from more than 80 areas along the Nankai Trough (e.g., Tsuji et al. 2002; Okamura and Matsuoka 2012; Kitamura et al. 2013); however, inter-regional correlation among these areas remains difficult because of sparse dates (Okamura and Matsuoka 2012) and discontinuities in the sedimentary record (Fujino et al. 2018; Tanigawa et al. 2018; Shimada et al. 2019). In this study, we obtained sediment cores containing a continuous record from 3000 years ago to the present day from Lake Kogare-ike, a coastal lake facing the central part of the Nankai Trough (Fig. 1). Application of X-ray computed topographic imaging and construction of Bayesian age–depth models for the sediment samples enabled us to recognize faint geological records of extreme wave events in historical and prehistoric time. The inundation history deduced in this study can provide new insights into inter-regional correlations with previously reported tsunami deposits along the Nankai Trough and contribute to the reconstruction of prehistoric and historic tsunami history.

2 Setting

2.1 Tectonics

Subduction-zone earthquakes occur repeatedly in the Nankai Trough, where the Philippine Sea plate is subducting beneath the Eurasian plate (Ishibashi 2004; Sangawa 2007; Usami et al. 2013; Fig. 1a). The coastal areas along the Nankai Trough are conventionally divided into six parts, Z and A–E (Fig. 1d) or, more simply, four segments (the Hyuga-nada segment, Z; the Nankai segment, A and B; the Tonankai segment, C and D; and the Tokai segment, E). Our study site is located in part C of the Tonankai segment. Instrumental and written records indicate that earthquakes have occurred with variable rupture zones and the associated tsunamis have inundated coastal areas in this region (Central Meteorological Observatory 1945; Ishibashi and Satake 1998; Fig. 1d). The latest two earthquakes on the Tonankai segment (the 1944 CE Showa-Tonankai and 1854 CE Ansei–Tokai earthquakes) caused coseismic coastal subsidence in the study area in Minami-ise town (Central Meteorological Observatory 1945; Hatori 1978; Education Center of Nanto Town 2000) (Fig. 1b). The geological record indicates that earthquakes and tsunamis have occurred along the Nankai Trough not only in the historical period but also over the past few thousand years (Garrett et al. 2016; Fujiwara et al. 2020a).

2.2 Historical records of extreme waves around the study site

2.2.1 Tsunamis

Instrumental records, written documents, tsunami monuments, and oral tradition record the latest three historical tsunamis associated with earthquakes along the Nankai trough: the 1944 CE Showa-Tonankai; the 1854 CE Ansei–Tokai; and the 1707 CE Hoei tsunamis (e.g., Editing Committee of the History of Nanto Town 1985;

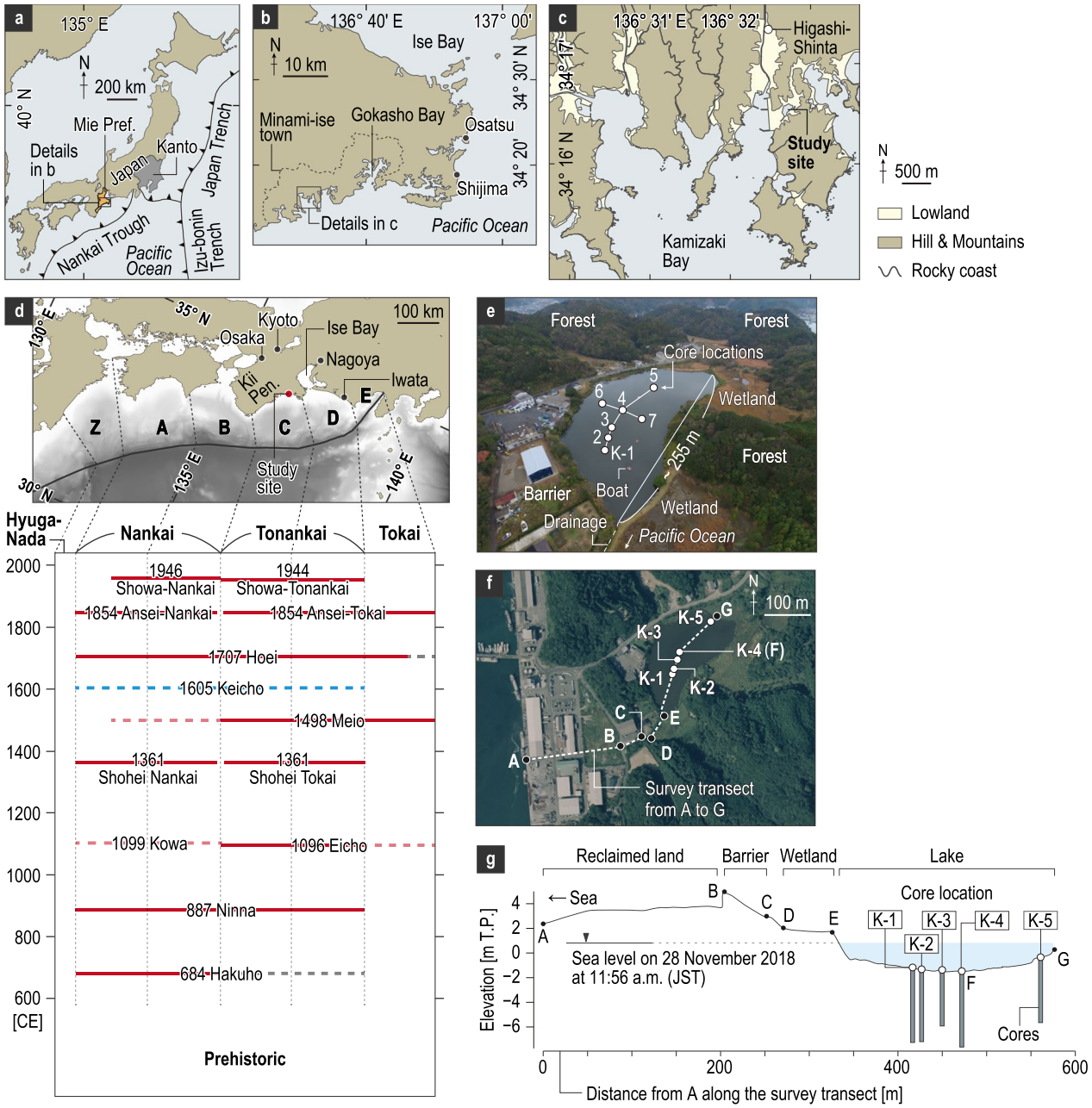

Fig. 1 **a** Index map of Japan. **b** Map of eastern Mie Prefecture showing the study site. **c** Location of the "Lake Kogare-ike" study site on the eastern shore of Kamizaki Bay. **d** Ages and estimated rupture zones of historical tsunamis along the Nankai Trough (modified from The Headquarters for Earthquake Research Promotion 2013). Red solid lines, red dotted lines, and gray dotted lines represent certain, probable, and possible rupture zones, respectively. The 1605 Keicho earthquake (dotted blue line) is regarded as a tsunami earthquake or an earthquake off an adjacent trench (Yamamoto and Hagiwara 1995; Seno 2002; Ishibashi and Harada 2013; Tsuji 2016). Generic Mapping Tools (Wessel et al. 2013) was partly used to create Fig. 1d. **e** Sediment sampling locations and topographic setting of the study site. The photograph was captured by an unmanned aerial vehicle. **f** Aerial photograph of the study site showing the survey transect from the shoreline (point A) to the inland end of Lake Kogare-ike (point G). The photograph was taken by the Geospatial Authority of Japan on 24 September 2008 (photograph number: CKK-2008-1X-C13A-13). **g** Topographic profile from the shoreline to the study site. Elevations are expressed with respect to mean sea level at Tokyo Bay (Tokyo Peil, T.P.)

Watanabe 1998; Education Center of Nanto Town 2000; Editing Committee of the History of Nansei Town 2004; Namegaya and Tsuji 2005). Instrumental records show that the wave height of the 1944 CE Showa-Tonankai tsunami was 5.4 m on the eastern shore of Kamizaki Bay (Editing Committee of the History of Nanto Town 1985;

Fig. 1c). Namegaya and Tsuji (2005) proposed, based on a local historical document, that the western shore of Kamizaki Bay was inundated by the 1854 CE Ansei–Tokai tsunami with a run-up height of 5.2 m Tokyo Peil (T.P.). They also estimated the run-up height of the 1707 CE Hoei tsunami on the eastern shore of Kamizaki Bay to have been 8.6 m, from an oral tradition that the tsunami reached Higashi-Shinta, approximately 1 km from the shoreline (Fig. 1c).

2.2.2 Storms

According to historical records, at least 55 storms attacked the area around Ise Bay (locally called "Isewan") between 1600 and 1865 CE (Arakawa et al. 1961; Fig. 1b, d; Additional file 1: Table S1). Instrumental records of wind directions, storm surges, and damage are available for storms since the mid-twentieth century. As many as 29 storms affected Mie Prefecture (Fig. 1a) between 1945 and 2017 CE (Japan Meteorological Agency 2017). The largest storm was the 1959 CE Isewan Typhoon, during which the highest storm surge in the observation history in Japan was recorded (Committees for Technical Investigation on Lessons Learned from Past Disasters 2008). The storm surge resulted in hazardous coastal inundation along Ise Bay and its surroundings. The inundation reached more than 15 km inland in the coastal areas north of Ise Bay (Fig. 1d) in association with a sea-level rise to 4.27 m T.P. (Japan Meteorological Agency 1961). Around the study site, sea level rose to 2.8 m T.P. and inundation extended more than 10 km inland at Gokasho Bay (Fig. 1b). According to one observation report, sea level rose to 2.3 m T.P. on the western shore of Kamizaki Bay (Editing Committee of the History of Nanto Town 1985; Fig. 1c).

2.3 Geomorphology

Coastal lakes and ponds are useful archives for reconstructing the long-term and continuous history of inundation by extreme waves (e.g., Sugawara et al. 2008; Baranes et al. 2016). These water bodies are usually stable depositional environments, in which coarser-grained event deposits sporadically emplaced by extreme waves are interbedded with muddy lacustrine sediments. Coastal wetlands such as swales and marshes are also commonly studied to identify event deposits (e.g., Atwater 1987; Cisternas et al. 2005; Pilarczyk et al. 2021; Okada et al. 2022), but coastal lakes/ponds have the advantage of a high preservation potential due to their stable, calm environment, and unfilled accommodation space (Szczuciński 2012; Kempf et al. 2017). This setting usually prevents event deposits from being completely eroded and yields reliable materials for dating.

Our study site was a coastal lake called Kogare-ike, which is isolated from the Pacific Ocean by a sand barrier (Fig. 1e, f). The height of the barrier is around 5 m T.P., though the maximum height is 4.8 m T.P. on the surveyed transect (Fig. 1f). Kamizaki Bay is a part of a complex ria-type coast, and the lake is surrounded by hills. The hills are composed of Upper Cretaceous pelitic mixed rock that includes blocks of basalt, chert, reddish siliceous mudstone, and sandstone (Nishioka et al. 2010). A narrow drainage channel connects the lake to the sea, but inflow and outflow are controlled by a sluice at present (Fig. 1e). The lake is more than 1 m deep in most parts and becomes deeper toward the center (Fig. 1f). The maximum depth is 2.3 m, and the elevation of the lake bottom at that point is approximately − 1.5 m T.P. The mean sea level at the study site is approximately equal to T.P.; the mean tide level at Owase, the nearest tide station to the study site, has been + 0.07 m T.P. for the past 10 years (from 2012 to 2021 CE) (Japan Meteorological Agency 2022a, 2022b). Agricultural activity around our study site can be recognized in the land use map for 1892, and aerial photographs show that farming was abandoned around 2003 (Additional file 2: Figure S1). This date is consistent with information from a landowner that the area of fringe marshes was used for agriculture before it was abandoned 10–15 years ago. There is no large freshwater input to the lake.

2.4 Previous studies on tsunami deposits in the study area

The inundation history at Lake Kogare-ike has not been explored previously, except for a preliminary study by Komatsubara et al. (2007), who collected three short (150-cm-long) cores from the lake bottom. They identified a sandy event deposit interbedded with muddy sediments by visual observation. A radiocarbon age of 980 ± 20 BP (recalibrated by this study to 958–791 cal BP) was obtained approximately 20 cm below the sand layer.

The geological evidence for earthquakes and tsunamis along the Nankai Trough has been summarized in a systematic review by Garrett et al. (2016). Here we summarize the geological record in areas adjacent to our study area, including reports published after Garrett et al. (2016). In the area east of our study site, tsunami deposits have been reported by Fujino et al. (2018) and Okahashi et al. (2005). Fujino et al. (2018) documented 10 sandy tsunami deposits dating to between 4500 and 500 cal BP in the Shijima lowland (Fig. 1b). The tsunami deposits were identified within muddy sediments by visual inspection and on X-ray radiographs. Three of these tsunami deposits were correlated with historical tsunamis (the 684 Hakuho tsunami, 1096 Eicho tsunami, and 1498 Meio tsunami). Okahashi et al. (2005) identified 12 tsunami deposits in a marsh at Osatsu (Fig. 1b) based on

sedimentary structures and micropaleontological evidence. They obtained radiocarbon ages from wood fragments and cones, but did not construct a chronology or estimate the depositional ages of each event deposit. To the west of our study site, Komatsubara et al. (2007) reported their preliminary results of stratigraphic observation of two short cores. They found 5–11 event deposits within peaty deposits at the Shihara lowland (Fig. 1d), but did not carry out detailed analysis of the samples.

3 Methods

3.1 Collection of sediment samples

We collected lacustrine sediments from seven locations at Lake Kogare-ike (K-1 to K-7; Fig. 1e, f) in 2018 and 2019. We assembled a raft with a hole in the center as a platform and pushed a 50-cm-long Russian sampler down to 4.75 m depth below the lake bottom. To recover continuous sedimentary records, we collected alternate overlapping samples from three or four different parallel holes. The holes were less than 1 m apart and overlaps of 25 cm were applied. In addition, push-core samples were obtained at K-1, K-4, and K-5 to recover soft surface sediments. The elevations of the ground surface and the present sea level were obtained with a network Real Time Kinematic-Global Navigation Satellite System (RTK-GNSS) survey system from Leica Geosystems Inc. (Norcross, Georgia, USA). The standard deviation (1 SD) of the leveling in our study was 0.005–0.017 m horizontally and 0.010–0.043 m vertically. The elevations of the lake bottom were obtained by subtracting the water depth measured with a leveling rod from the elevation of the lake surface measured with RTK-GNSS.

3.2 Observation and grain size analysis of sediment samples

We observed the collected sediment samples in both the field and the laboratory. In the laboratory, X-ray computed tomography (CT) scans of the cores were obtained with a Hitachi Supria Grande Premium CT scanner (Hitachi, Ltd., Tokyo, Japan) at the Geological Survey of Japan (Tsukuba, Ibaraki, Japan). The CT images were referred to during visual observation and used to guide subsampling for radiocarbon dating, gamma-ray spectrometry, grain size analysis, and diatom assemblage analysis.

Grain size analyses of the samples were conducted using a Retsch Camsizer (Verder Scientific, Haan, Germany), an image analyzer capturing a wide range of grain size from silt to pebbles. All samples were sieved in water to remove the mud component and then treated with hydrogen peroxide solution to remove the organic components. During the procedure, large pieces of organic matter (roots, leaves, and wood fragments) were removed by hand. The sand content of each sample was calculated from the resulting weight reduction. The measurement range of grain size analysis on the residual sand fractions was set from −5.25 to +6.25 phi at intervals of 0.25 phi. Grain size distribution properties were calculated using the logarithmic graphical method of Folk and Ward (1957).

3.3 Analysis of volcanic glass shards

The elemental concentrations of volcanic glass shards in event deposit E11 at locations K-3, K-4, K-6, and K-7 were measured with an energy dispersive X-ray microanalyzer (EDX) by Furusawa Geological Survey Inc., Okazaki, Japan. Identification of glass sources was carried out by referring to previously published regional studies (Sugihara 1984; Machida and Arai 2003; Sugiuchi and Fukuoka 2005; Tsukui et al. 2006; Kobayashi et al. 2020; Murata et al. 2021).

3.4 Diatom analysis

Fossil diatom assemblages in 127 samples from the core from K-4 were studied to reconstruct the paleoenvironment of the study site. The samples were prepared by the bleaching method (Nagumo and Kobayasi 1990; Nagumo 1995). Fossil diatoms were identified under an optical microscope. More than 200 valves were counted per sample. Identification and ecological information followed standard (e.g., Patrick and Reimer 1966, 1975; Simonsen 1987; Krammer and Lange-Bertalot 1986, 1988, 1991a, b) and regional (Kosugi 1988; Kobayasi et al. 2006) sources. Fossil diatoms were divided into seven groups on the basis of their autoecology: freshwater plankton, freshwater–brackish plankton, freshwater tychoplankton, freshwater benthos, freshwater–brackish benthos, brackish benthos, and unknown.

Stratigraphically constrained cluster analysis (Grimm 1987) was performed to statistically identify the zonation of fossil diatom assemblages. The cluster analysis was carried out using the Bray–Curtis distance among the assemblages and constraining the stratigraphic order of the samples. The cluster analysis was executed using the package "rioja" in R version 4.2.2 (Juggins 2022).

3.5 Radiocarbon dating, gamma spectrometry, and Bayesian age–depth modeling

Radiocarbon dating of plant macrofossils and fossil pollen grains was conducted to estimate depositional ages. Macrofossils were selected under a binocular microscope. Fossil pollen grains were extracted from sediment samples at the Research Centre for Palaeoclimatology, Ritsumeikan University (Kusatsu, Shiga, Japan) following the procedure of Yamada et al. (2021). Radiocarbon dating of plant macrofossils and pollen grains was carried

out by Beta Analytic (Miami, Florida, USA) and the University of Tokyo (Tokyo, Japan), respectively.

Cesium-137 activities of 29 samples from shallower than 140 cm depth in the sediment core collected at K-4 were measured by high-resolution gamma spectrometry (GCW2022; Mirion Technologies [Canberra], Inc, Meriden, Connecticut, USA). Cesium-137 is one of the most common radionuclides used to establish chronologies for sediments during the last 80 years. Cesium-137 is an anthropogenic radionuclide that was produced by atmospheric nuclear weapons testing from 1950 to ~1975. In the northern hemisphere, undisturbed sedimentary records generally show the first occurrence (onset) and the peak of ^{137}Cs as time markers for 1954 and 1963–1964, respectively (Ritchie and McHenry 1990; Appleby 2001), though ^{137}Cs onset might have occurred earlier in western Japan than in other regions in the northern hemisphere because of the nuclear bomb attacks on Hiroshima and Nagasaki in World War II (see discussion).

A Bayesian age–depth model of the sediments at K-4 was constructed based on the radiocarbon ages. We applied Bchron (Haslett and Parnell 2008; Parnell et al. 2008), a package written for the free open-source language R (R Core Team 2021). Age–depth models were constructed by using IntCal20 (Reimer et al. 2020) as the radiocarbon calibration curve. Event deposits were treated as instantaneous, and their thicknesses were removed from the original core log of K-4 to construct an event-free stratigraphic column (Kempf et al. 2017, 2020; Sabatier et al. 2017). For this reason, the radiocarbon age measured within event deposit E1 (no. 20 in Table 1) was not used in the age–depth model. Because of the stochastic nature of the Bchron model, which uses random sampling, each run produces slightly different depositional ages; therefore, the depositional ages of event deposits E1–E19 were determined by averaging the ages obtained from the three trials.

Table 1 Radiocarbon ages from the study site

No.	Core location	Elevation (m T.P.)	Position	Conventional age (^{14}C BP)	Calibrated age 2σ range (cal BP)	Calibrated age 2σ range (cal CE/BCE)	Material	Lab no.
1	K-1	− 2.51 to − 2.45	Between E3 and E4	304 ± 34	461–295	1489–1655 CE	Concentrated pollen	TKA-23301
2	K-1	− 2.98 to − 2.94	Below E5	777 ± 33	730–668	1220–1282 CE	Concentrated pollen	TKA-23296
3	K-1	− 3.73 to − 3.69	Above E7	590 ± 30	647–540	1303–1410 CE	Leaves, *Cladium chinense*, and seeds of unidentified taxa	Beta-581028
4	K-1	− 4.05 to − 4.01	Between E7 and E8	870 ± 30	901–690	1049–1260 CE	A leaf of unidentified taxon	Beta-581029
5	K-1	− 4.45 to − 4.43	Below E9	1130 ± 30	1174–958	776–992 CE	*Najas* spp., *Potamogeton* spp., *Trapa* spp., and unidentified taxa	Beta-531173
6	K-1	− 4.85 to − 4.81	Below 10	1430 ± 30	1367–1294	583–656 CE	Leaves and seeds of unidentified taxa	Beta-581030
7	K-1	− 5.06 to − 5.04	Above E13	1720 ± 30	1700–1539	250–411 CE	Fruits of unidentified taxa	Beta-531172
8	K-1	− 5.39 to − 5.35	Below E14	1841 ± 36	1829–1627	121–323 CE	Concentrated pollen	TKA-23290
9	K-2	− 2.08 to − 2.06	Above E2	150 ± 30	282–0	1668–present	Branch	Beta-531171
10	K-2	− 2.53 to − 2.50	Below E3	273 ± 50	475–0	1475–present	Concentrated pollen	TKA-23294
11	K-2	− 3.27 to − 3.24	Between E5 and E6	624 ± 33	655–551	1295–1399 CE	Concentrated pollen	TKA-23302
12	K-2	− 3.94 to − 3.90	E7	470 ± 30	541–492	1409–1458 CE	Leaves and seeds of unidentified taxa	Beta-581031
13	K-2	− 4.18 to − 4.14	Below E7	1100 ± 30	1062–933	888–1017 CE	Leaves and seeds of unidentified taxa	Beta-581032

Table 1 (continued)

No.	Core location	Elevation (m T.P.)	Position	Conventional age (^{14}C BP)	Calibrated age 2σ range (cal BP)	Calibrated age 2σ range (cal CE/BCE)	Material	Lab no.
14	K-2	− 4.68 to − 4.65	Above E9	1290 ± 30	1290–1154	660–796 CE	Leaf	Beta-583061
15	K-2	− 4.81 to − 4.77	Between E9 and E10	1330 ± 30	1300–1177	650–773 CE	Leaves and seeds of unidentified taxa	Beta-581033
16	K-2	− 5.28 to − 5.23	Above 12	560 ± 30	640–524	1310–1426 CE	Leaves and seeds of unidentified taxa	Beta-581034
17	K-3	− 3.41 to − 3.36	Above E5	780 ± 30	729–672	1221–1278 CE	Najas spp., Seeds of unidentified taxa, a fruit of unidentified taxon, and leaves	Beta-664442
18	K-3	− 3.55 to − 3.51	Below E6	900 ± 30	908–732	1042–1218 CE	Seeds of unidentified taxa, leaves	Beta-665871
19	K-3	− 4.59 to − 4.55	Between E10 and E11	1490 ± 30	1404–1309	546–641 CE	Leaves, *Cladium chinense*, and seeds of unidentified taxa	Beta-583062
20	K-4	− 2.09 to − 2.05	Within E1	287 ± 28	446–158	1504–1792 CE	Concentrated pollen	TKA-23297
21	K-4	− 2.72 to − 2.68	Above E2	209 ± 37	311–0	1639–present	Concentrated pollen	TKA-23298
22	K-4	− 3.09 to − 3.05	Below E3	303 ± 32	458–295	1492–1655 CE	Concentrated pollen	TKA-21913
23	K-4	− 3.33 to − 3.34	Below E5	260 ± 30	435–0	1515–present	*Trapa* spp.	Beta-545282
24	K-4	− 3.46 to − 3.42	Between E5 and E6	653 ± 38	670–555	1280–1395 CE	Concentrated pollen	TKA-24604
25	K-4	− 3.59 to − 3.55	Below E6	901 ± 45	915–729	1035–1221 CE	Concentrated pollen	TKA-21914
26	K-4	− 3.9 to − 3.88	Below E7	820 ± 30	782–678	1168–1272 CE	Leaves and seeds of unidentified taxa	Beta-528350
27	K-4	− 4.05 to − 4.00	Above E8	660 ± 30	670–557	1280–1393 CE	Leaves	Beta-545283
28	K-4	− 4.06 to − 4.02	Above E8	1371 ± 27	1344–1179	606–771 CE	Concentrated pollen	TKA-24607
29	K-4	− 4.28 to − 4.23	Between E8 and E9	1292 ± 39	1294–1126	656–824 CE	Concentrated pollen	TKA-21911
30	K-4	− 4.36 to − 4.35	Below E9	1300 ± 30	1289–1177	661–773 CE	Leaves	Beta-528349
31	K-4	− 4.54 to − 4.51	Below E10	1490 ± 30	1404–1309	546–641 CE	Leaves	Beta-528351
32	K-4	− 4.75 to − 4.69	Between E11 and E12	1540 ± 30	1516–1353	434–597 CE	Leaves and seeds of unidentified taxa	Beta-545279
33	K-4	− 4.84 to − 4.82	Above E12	1480 ± 30	1398–1308	552–642 CE	Leaves, branch, and fruits of unidentified taxa	Beta-528352
34	K-4	− 5.03 to − 5.02	Below E14	1650 ± 30	1687–1414	263–536 CE	Branch	Beta-528353
35	K-4	− 5.14 to − 5.03	Below E14	1500 ± 30	1466–1308	484–642 CE	Leaves	Beta-528354
36	K-4	− 5.23 to − 5.17	Between E14 and E15	1980 ± 30	1991–1831	41 BCE–119 CE	Fruits or seeds of an unidentified taxon	Beta-545280
37	K-4	− 5.33 to − 5.28	Above E15	2040 ± 27	2098–1891	148 BCE–59 CE	Concentrated pollen	TKA-24606
38	K-4	− 5.60 to − 5.57	Between E15 and E16	2420 ± 30	2695–2352	745–402 BCE	*Najas* spp., Fruits of unidentified taxa, and leaves	Beta-545281

Table 1 (continued)

No.	Core location	Elevation (m T.P.)	Position	Conventional age (^{14}C BP)	Calibrated age 2σ range (cal BP)	Calibrated age 2σ range (cal CE/BCE)	Material	Lab no.
39	K-4	− 5.70 to − 5.66	Below E16	2598 ± 40	2836–2516	886–566 BCE	Concentrated pollen	TKA-23299
40	K-5	− 2.41 to − 2.37	Below the 3rd shallowest event deposit	319 ± 30	461–306	1489–1644 CE	Concentrated pollen	TKA-23300
41	K-5	− 3.07 to − 3.03	Below the 3rd deepest event deposit	411 ± 35	522–326	1428–1624 CE	Concentrated pollen	TKA-23289
42	K-5	− 4.22 to − 4.18	Below E8	970 ± 30	928–798	1022–1157 CE	Leaves of Dicotyledoneae sp.	Beta-581027
43	K-5	− 4.55 to − 4.50	Below the deepest event deposit	1567 ± 37	1523–1383	427–567 CE	Concentrated pollen	TKA-23292
44	K-6	− 3.57 to − 3.52	Below E5	620 ± 30	651–551	1299–1399 CE	Seeds of unidentified taxa, and leaves	Beta-664440
45	K-6	− 5.16 to − 5.12	Above E12	1310 ± 30	1293–1177	657–773 CE	Leaves	Beta-664441
46	K-7	− 3.96 to − 3.92	Above E8	720 ± 30	719–568	1231–1382 CE	Seeds of unidentified taxa, a fruit of unidentified taxon, and leaves	Beta-664438
47	K-7	− 5.43 to − 5.39	Below E14	1820 ± 30	1821–1624	129–326 CE	*Najas* spp., Seeds of unidentified taxa	Beta-664439

Conventional ages were converted to cal BP with Bchron (Haslett and Parnell 2008; Parnell et al. 2008) using the calibration curve of IntCal20 (Reimer et al. 2020)

4 Results

4.1 Stratigraphy and ages of sediment samples from Kogare-ike

4.1.1 Detailed description of the stratigraphy at the center of the lake

The sediments from Lake Kogare-ike were composed of organic mud, sand, gravel, inorganic mud, and volcanic ash. Sand, sandy mud (with/without gravel), inorganic mud, and white volcanic ash layers were observable with the naked eye both in the field and in the laboratory as distinctive layers interbedded with organic mud. In addition to these, there were 10 high-radiodensity layers that could be recognized only in X-ray CT images. The high-radiodensity layers possibly possessed different mineral compositions (Boespflug et al. 1995) or larger grain size (Godbout et al. 2019) than the organic mud layers. We regard these sand, sandy mud, inorganic mud clasts, volcanic ash, and high-radiodensity layers as event deposits (Figs. 2, 3 and 4; Additional file 3: Figure S2, Additional file 4: Figure S3, and Additional file 5: Figure S4; Additional file 6: Table S2) and have named them E1–E19 from top to bottom. Details of each event deposit at K-4 are described in the following paragraphs. Details of the contents of mud, organic material, and sand and the results of grain size analysis in each layer are provided in Fig. 4 and Additional file 7: Table S3.

E1, the uppermost event deposit, was gray in color and ranged from 46.9 to 77.1 cm core depth. This event deposit was visible as a stack of three subunits both to the naked eye and in the CT images (Fig. 4). We could not recognize an erosional lower contact with the underlying organic mud in the CT images. Parallel laminae were distinct within the subunits. The sand content of E1 was between 0.9 and 3.4 wt.% (Fig. 4 and Additional file 7: Table S3).

E2 appeared as a grayish faint inorganic mud layer to the naked eye, and was visible as a high-radiodensity layer from 140.0–141.8 cm depth in the CT images (Fig. 4). The sand content was low (< 1 wt.%) above, below, and within event deposit E2 (Fig. 4 and Additional file 7: Table S3).

E3 was a sandy layer at 153.6–156.2 cm core depth. The lower part of E3 consisted of medium sand (mean grain size = 1.55 ϕ). The upper part of the event deposit contained multiple layers of gray inorganic mud and brown organic mud. Changes in the sand contents show grading in grain size of this event deposit. The upper part was difficult to recognize with the naked eye but was clear on the CT images (Fig. 4).

E4 and E5 were recognized as high-radiodensity layers only on the CT images at 172.9–173.8 cm and 183.9–184.5 cm core depth, respectively. Event deposit E4 showed very faint lateral continuity within the core. The

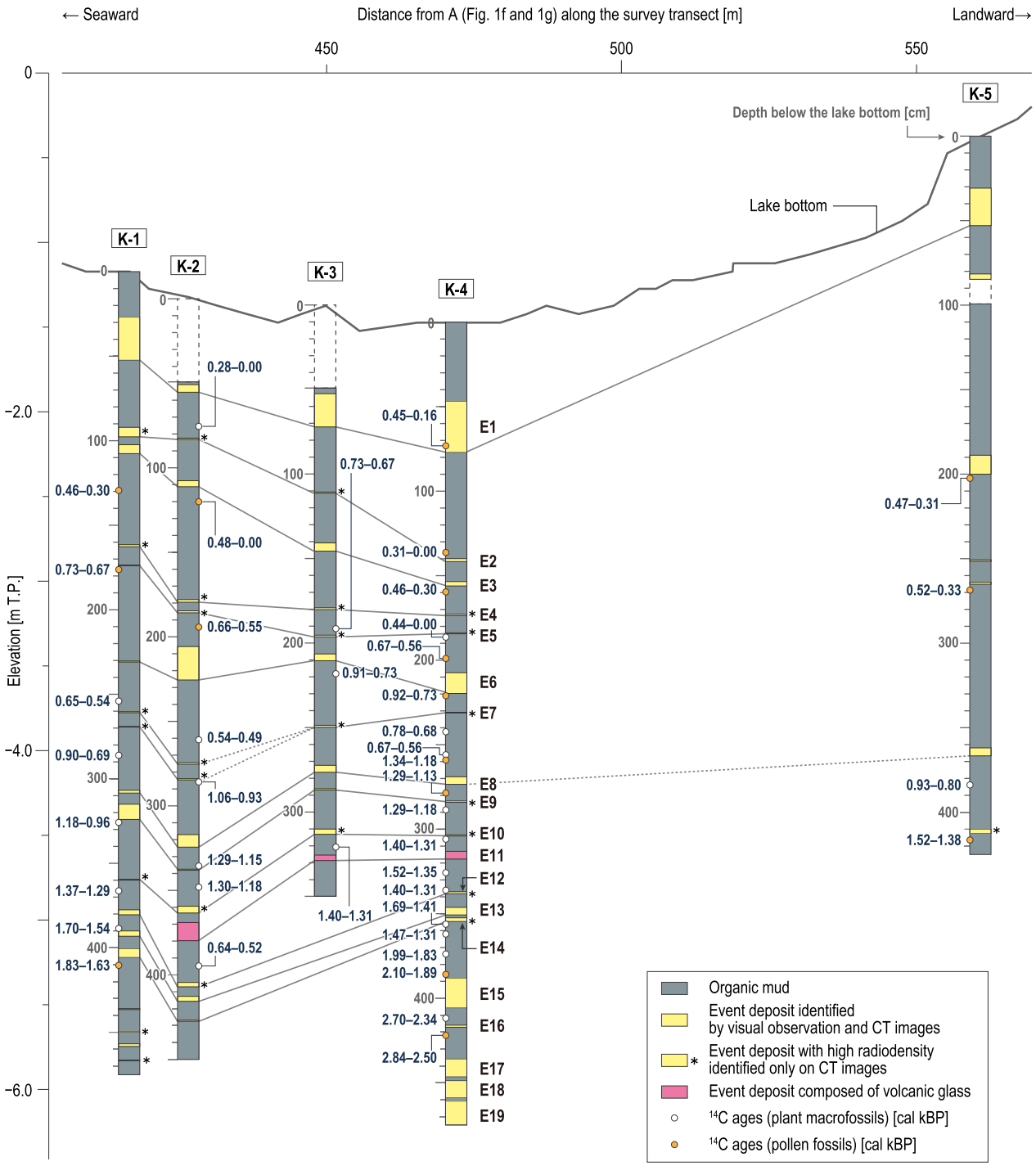

Fig. 2 Lithostratigraphy from K-1 to K-5 (locations in Fig. 1e). Radiocarbon ages are listed in Table 1. The correlations of event deposits between core sites are shown as solid lines, with tentative correlations indicated by dotted lines. Stacks of X-ray CT images are shown on Additional file 3: Figure S2 and Additional file 4: Figure S3. A photograph of the core from K-4 is provided in Additional file 3: Figure S2

sand contents of the two event deposits were less than 1 wt.% above, below, and within the layers (Fig. 4 and Additional file 7: Table S3).

E6 occurred between 207.5 and 219.8 cm core depth. As shown in the CT images, this event deposit was not clearly divided into subunits, in contrast to the younger

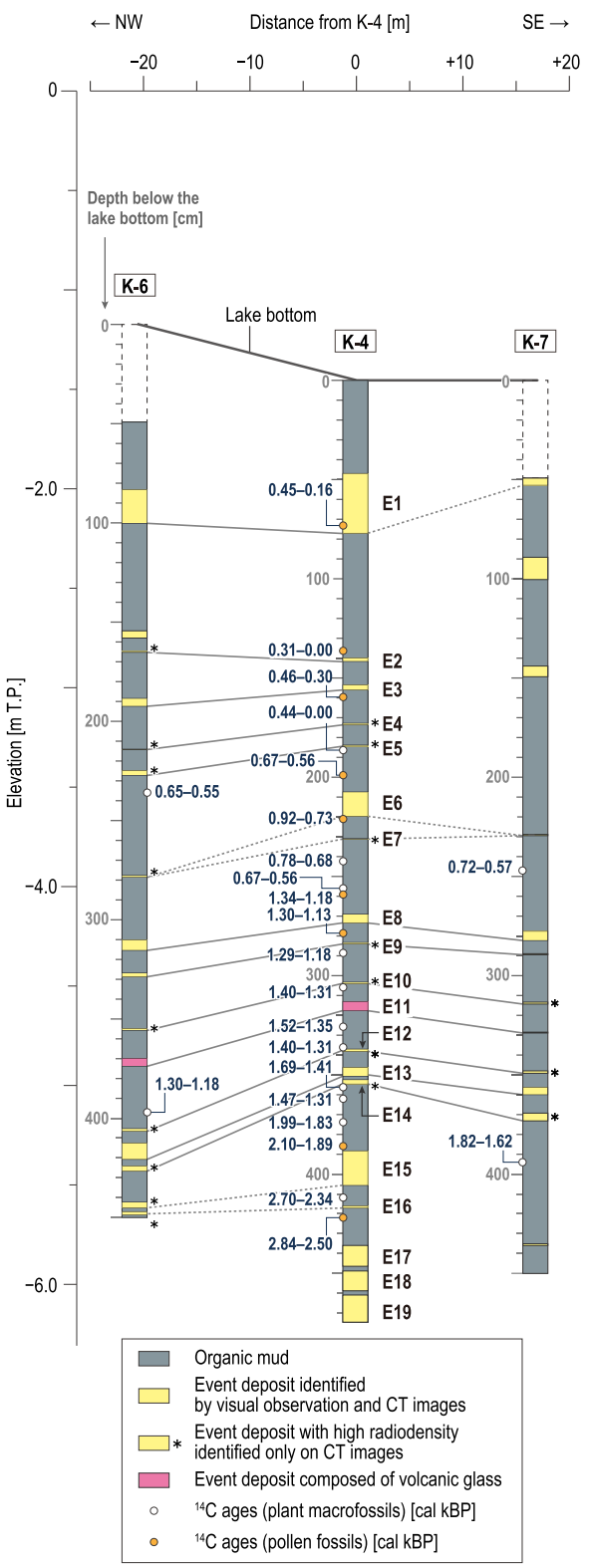

Fig. 3 Lithostratigraphy of a transect connecting K-6, K-4, and K-7 (locations in Fig. 1e). Radiocarbon ages are listed in Table 1. The correlations of event deposits between core sites are shown as solid lines, with tentative correlations indicated by dotted lines. Stacks of X-ray CT images are shown on Additional file 3: Figure S2 and Additional file 4: Figure S3. A photograph of the core from K-4 is provided in Additional file 3: Figure S2

events. It was difficult determine from visual observation and CT images whether the non-layered structure of E6 was created by obvious bioturbation or deformation of the sand layer after rapid deposition (e.g., load casting). The sand content of E6 ranged from 10.5 to 31.2 wt.%. E6 contained a small proportion of granules, but the mean grain size of the sieved residual sand fractions was fine–coarse sand (2.49–0.25 ϕ, average = 1.17 ϕ). The sand content and the results of grain size analyses show grading within the event layer.

A faint event deposit (E7) at 231.0–231.3 cm core depth was recognized only on CT images. This deposit was visible as a rather patchy horizontal distribution within the core, rather than a stratified high-radiodensity layer. The sand content was low (less than 1 wt.%) above, below, and within event deposit E7.

E8 was a light grayish inorganic mud layer between 269.1 and 273.6 cm core depth. A few mud clasts were recognized both in the field and on CT images at the base of the event deposit. The CT images showed an upward change in radiodensity from high to low, which may represent upward fining of grain size; however, no grading was recognized in the sand content or grain size analysis.

E9 and E10 were visible only on the CT images at 283.4–284.3 cm and 303.4–304.2 cm core depth, respectively. The two layers exhibited high radiodensity and were distinctively stratified on the images, but there was no significant change in the sand content (< 1 wt.%) or the grain size of the residual sand fractions.

E11 appeared at 313.3–317.9 cm core depth. The bottom part of the event deposit was a very distinctive white layer in the field. The middle and upper parts of the layer were hard to recognize with the naked eye but visible on the CT images. This event layer consisted of pumice and glass shards. EDX analyses indicated that the shards had various origins (see below), suggesting erosion and redeposition from older strata.

A faint event deposit, E12, was visible only on CT images at 337.2–338.4 cm core depth. This event deposit was apparent as a patchy distribution within the core, and the sand content of the sediment was less than 1 wt.% above, below, and within the event deposit.

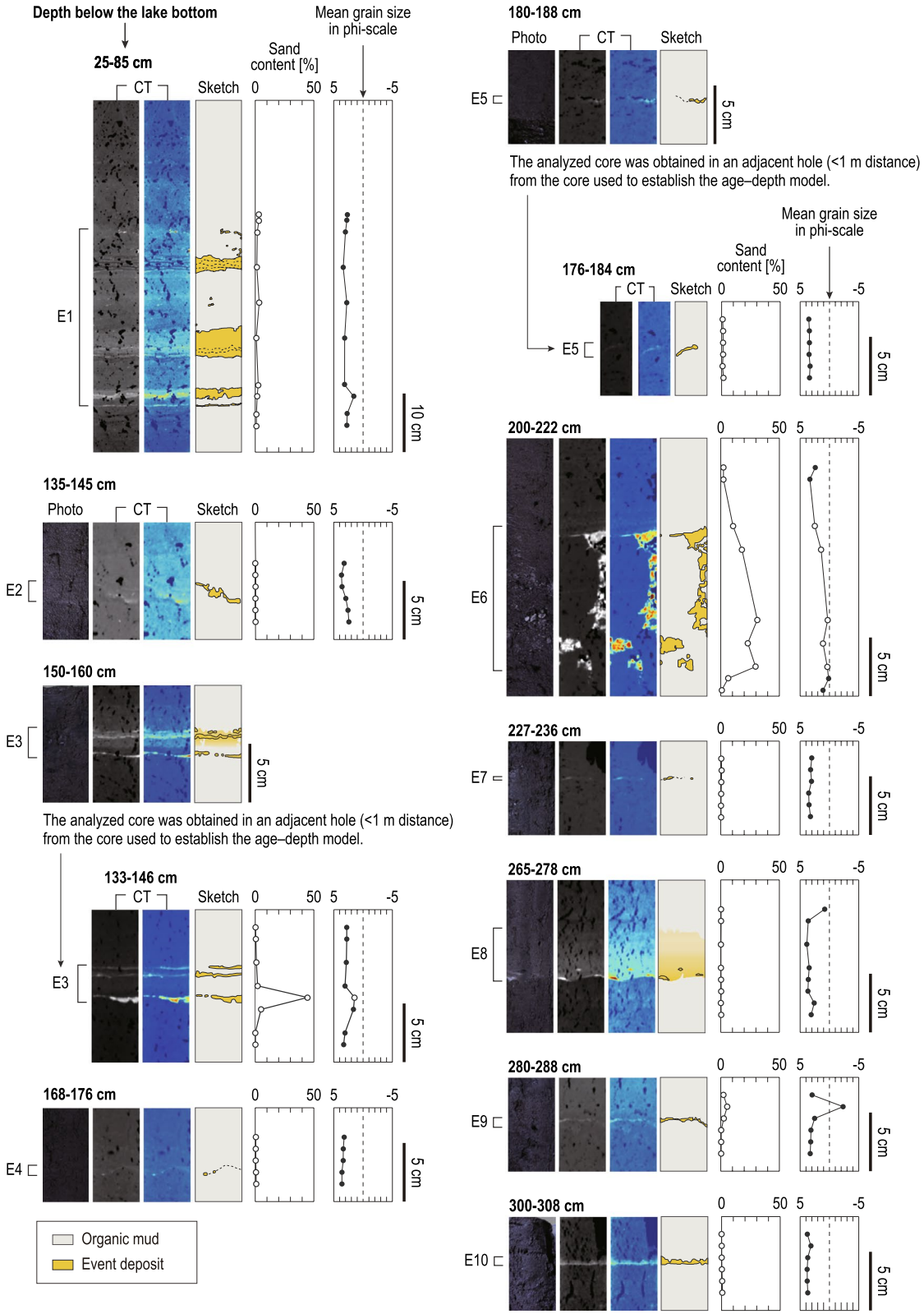

Fig. 4 Photographs, X-ray CT images, and sketches of the event deposits identified at K-4 with the results of grain size analysis (sand content and mean grain size of residual sand fractions). The mean grain size, shown as black circles, represents that of samples with very small sand contents (10% or less)

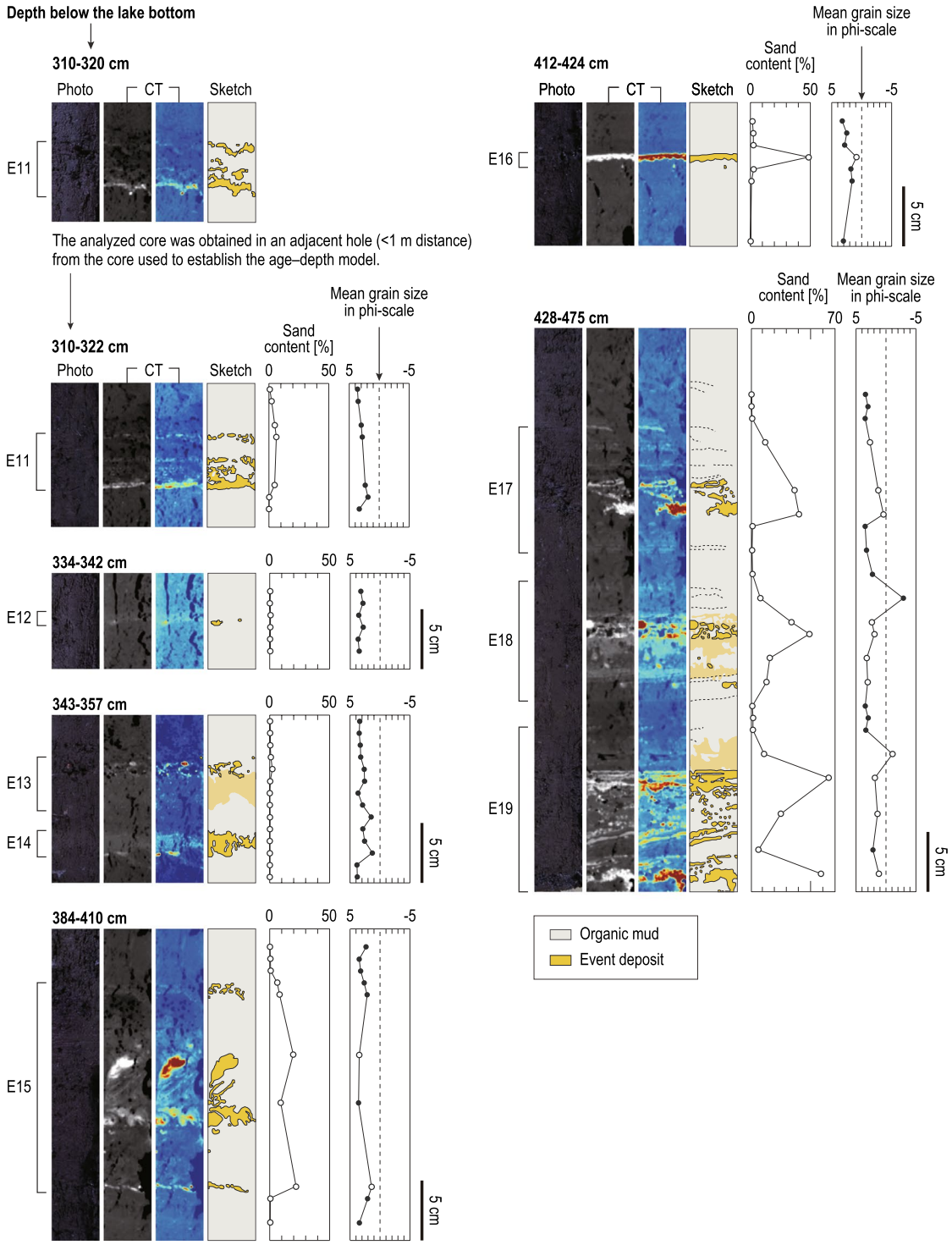

Fig. 4 continued

E13 was distributed at 346.5–350.9 cm core depth. To the naked eye, the upper part of the event layer was visible as a light grayish inorganic mud layer. The upper part had higher density than the lower part in the colored CT image. There was no significant difference in sand content between the upper and lower parts.

E14 was identified only on the CT images, and occurred between 352.6 and 354.8 cm core depth. The CT images

showed higher radiodensity at the bottom of the layer than in the middle and upper parts, but no difference was recognizable with the naked eye. The sand content was persistently low (less than 1 wt.%) above, below, and within the event deposit.

E15 occurred between 388.5 and 406.0 cm core depth. The CT images showed three sandy and muddy subunits within the event deposit. The middle subunit appeared not to be stratified, but we could not determine whether the lack of strata was caused by bioturbation or load casting. The sand contents and grain size analyses of the subunits indicated that the lowest subunit contained much more sand and coarser fractions than the higher subunits. The mean grain size of the uppermost, middle, and lowest subunits was fine sand (mean grain size is 2.68–2.12 ϕ), very fine sand (mean grain size = 3.57–3.45 ϕ), and medium sand (mean grain size = 1.37 ϕ), respectively. Debris filled the space between the upper and middle subunits. The lower contact with the underlying deposit was sharp (less than 5 mm).

E16 was visible to the naked eye as a distinct grayish sandy layer at 416.2–417.4 cm core depth. The sand content and mean grain size of the event were 48.5 wt.% and coarse sand (mean grain size = 0.85 ϕ), respectively. The upper and lower contacts with the overlying and underlying deposits were sharp.

E17 was a grayish sandy mud layer at 436.2–446.7 cm core depth. The CT images showed clear parallel laminae in the upper and basal parts of the event deposit. The sand content in the basal part of the event deposit was low sand content (< 1 wt.%), whereas the upper three samples within the event deposit showed relatively high sand content (11.6 to 39.7 wt.%). The mean grain size of the residual sand fractions of the upper three samples was fine–coarse sand (2.72– 0.53 ϕ, 1.52 ϕ on average). The sand contents and mean grain size indicated upward fining of grain size. The well-preserved clear laminae may suggest that this event layer had not been vertically disturbed, for example, by benthic fauna, after deposition.

E18 was recognized as a grayish sandy mud layer at 449.1–459.1 cm core depth. The CT images enabled us to recognize clear laminae in the upper and lower parts of the layer. The sample in the upper part had low sand content (7.5 wt.%). The sand contents in other four samples ranged from 12.6 to 48.4 wt.%. The mean grain size of the residual sand fractions in these four samples was very fine to medium sand (1.79 to 3.22 ϕ, average 2.57 ϕ). The CT images and changes in the sand content and mean grain size indicated inverse and normal grading within the event layer.

The lowest event deposit, E19, was a gray distinctive layer that consisted of sandy mud, muddy sand, and granules. The CT images showed laminae, visible as high-radiodensity layers. The sand content was 1.2–64.4 wt.%. Grain size analyses showed that the residual sand fractions were in the medium sand range (mean grain size of the four samples with a sand content of more than 10% = 1.08 phi). The top of E19 was observed at 461.3 cm core depth, but the bottom was not clearly confirmed in our fieldwork.

4.1.2 Major-element composition of volcanic glass shards

The major-element compositions of individual glass shards from the volcanic ash layer (event deposit E11) showed various sources and ages of eruptions (Additional file 8: Fig. S5). Major elements, especially MgO, CaO, Na_2O, and K_2O, are useful to distinguish the sources of volcanic ash layers around the study site (Sugihara 1984; Machida and Arai 2003; Kobayashi et al. 2020; Murata et al. 2021). Scatter plots of MgO–SiO_2, CaO–SiO_2, Na_2O–SiO_2, and K_2O–SiO_2 for volcanic ash corresponding to E11 in four cores (K-3, K-4, K-6, and K-7) recognized four clusters of element compositions. Three of the clusters correspond to widespread tephras; specifically, the Aira-Tn tephra (AT; 29–26 cal kBP), the Kikai-Akahoya tephra (K-Ah; 7.3 cal kBP), and the Amagi-Kawagodaira tephra (Kg; 3.1 cal kBP) (Sugihara 1984; Machida and Arai 2003). The other cluster is similar to the element composition of Izu Island eruptions (low CaO and high Na_2O and K_2O), especially the Kozushima-Tenjosan tephra (Iz-Kt; AD 838) (Sugihara 1984; Sugiuchi and Fukuoka 2005; Tsukui et al. 2006; Kobayashi et al. 2020; Murata et al. 2021), though this age exhibits a discrepancy with the radiocarbon dating.

4.1.3 Dating by radioactive isotopes

The obtained radiocarbon ages ranged from 2836–2516 to 282–0 cal BP (Figs. 2 and 3; Table 1). Forty-seven radiocarbon ages were obtained, 30 of which were from plant macrofossils and the remaining 17 from concentrated pollen fossils.

Cesium-137 was detectable in samples above 93 cm in depth at K-4, but its concentration in deeper samples was below the detection limit (Fig. 5 and Additional file 9: Table S4). The concentration of ^{137}Cs ranged from 0.8 ± 0.2 to 1.9 ± 0.2 Bq/kg in samples between 93 cm and 82.5 cm core depth (below E1), but exhibited a pronounced increase just above E1. The highest ^{137}Cs concentration was recognized at 42.5 cm depth below the lake bottom (28.5 ± 0.6 Bq/kg). Thereafter, the

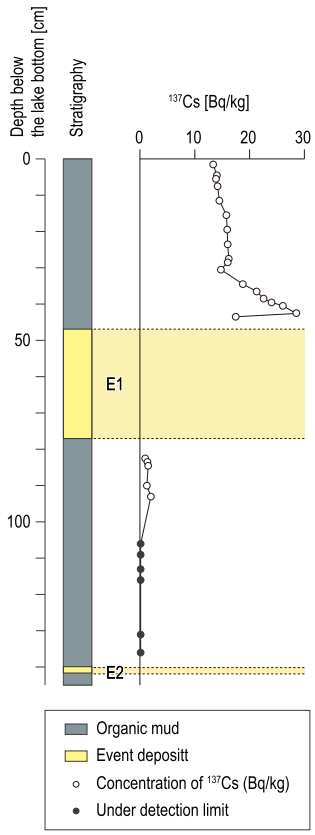

Fig. 5 The ^{137}Cs profile in the top of the core from K-4. Details of the analytical results are listed in Additional file 9: Table S4

concentration decreased consistently upward, except for a slight increase from 30.5 to 27.5 cm core depth.

4.1.4 Intra-site correlation of event deposits among cores taken from Kogare-ike

The stratigraphic features and positions of event deposits, chemical composition of glass shards, and radiocarbon ages permitted us to correlate event deposits E1–E16 at K-4 with event deposits in the cores taken from the other six locations at Kogare-ike (K-1, K-2, K-3, K-5, K-6, and K-7; Figs. 2 and 3). No event deposits correlative with E17–E19 were present in any cores except for K-4, because of short recovery of the sediment cores taken from K-1, K-2, K-3, K-5, K-6, and K-7. The correlations of the other events (E1–E16) are described below; the characteristics of each event are summarized in Additional file 6: Table S2.

Event deposit E1 found at K-4 correlated among K-1–K-6 and possibly K-7. The correlation is made on the basis of the depth of the lower contact of the event at K-1–K-7 (about 50–100 cm from the lake bottom) and the stratigraphic features at K-1 and K-3–K-6 (multiple subunits of high radiodensity and parallel laminae).

Event deposits E2 and E3 at K-4 were found at K-1–K-4 and K-6. The two event deposits were present in organic mud younger than 461–295 cal BP (no. 1 in Table 1) at K-1 and within organic mud dated between 282 and 0 cal BP (no. 9 in Table 1) and 475–0 cal BP (no. 10 in Table 1) at K-2 and 311–0 cal BP (no. 21 in Table 1) and 458–295 cal BP (no. 22 in Table 1) at K-4. Two event layers at each of K-3 and K-6 were correlated with E2 and E3 on the basis of their depth and stratigraphic features: E2 is a very faint layer and E3 has multiple laminae with high radiodensity.

Event deposits E4 and E5 were correlated among K-1–K-4 and K-6. The two events are located within organic mud dated between 461 and 295 cal BP (no. 1 in Table 1) and 730–668 cal BP (no. 2 in Table 1) at K-1, between 475 and 0 cal BP (no. 10 in Table 1) and 655–551 cal BP (no. 11 in Table 1) at K-2, and between 458–295 cal BP (no. 23 in Table 1) and 670–555 cal BP (no. 25 in Table 1) at K-4. The correlations are also based on a radiocarbon age between E4 and E5 at K-3 (729–672 cal BP, no. 17 in Table 1) and a limiting maximum age of E5 at K-6 (651–551 cal BP, no. 44 in Table 1). These deposits' stratigraphic features (i.e., a very thin layer, or visible only on CT images) are consistent among the cores.

Event deposit E6 of K-4 can probably be correlated with event deposits at K-1–K-3, and possibly K-6 and K-7. This correlation is based on stratigraphic features, depths of event layers, and three radiocarbon ages. Stratigraphic features visible as multiple layers of high radiodensity in the CT images are very similar between event layers at K-2 and K-3. However, high-radiodensity layers correlative to deposit E6 are very thin at K-1. We correlated event deposit E6 of K-4 with those of K-1–K-3 on the basis of the depths of the event deposits and four radiocarbon ages (655–551 cal BP, no. 11 in Table 1; 908–732 cal BP, no. 18 in Table 1; 670–555 cal BP, no. 24 in Table 1; and 915–729 cal BP, no. 25 in Table 1).

A faint event deposit, E7, is found at K-1–K-4, and possibly K-6 and K-7. The depositional age of E7 at K-4 is constrained by three limiting maximum ages (782–678 cal BP, no. 26 in Table 1; 670–557 cal BP, no. 27 in Table 1; and 1344–1179 cal BP, no. 28 in Table 1) obtained from samples below the event deposit E7 and a limiting minimum age (915–729 cal BP; no. 26 in Table 1) from a sample above E7. At K-1 and K-2, two high-radiodensity layers correspond to the constrained age of E7 at K-4. Either of these two layers may be correlated with E7 of K-4; alternatively, the two high-radiodensity layers may represent a single event such as a single tsunami deposit having multiple subunits due to multiple waves. Event layers at depths of ~ 284 cm at K-6 and ~ 229 cm at K-7 are possibly correlated either E6 or E7 based on their

depths on CT images and stratigraphic position above the light grayish inorganic mud layer (E8).

Event deposit E8 was correlated among K-1–K-4, K-6, and K-7 by means of sedimentary features (light grayish inorganic mud and mud clasts). Radiocarbon ages from samples above E8 at K-1 (901–690 cal BP, no. 4 in Table 1) and below E8 at K-2 (1290–1154 cal BP, no. 14 in Table 1) is consistent with this visual correlation. An event deposit at 362.1–367.0 cm depth at K-5 may also correlate with E8, but an age from a sample below the event (928–798 cal BP, no. 42 in Table 1) is younger than event deposit E8 at K-4.

Event layers corresponding to event deposit E9 at K-4 were found at K-1, K-2, K-3, K-6, and K-7. The depositional age of E9 at K-4 is constrained by a limiting maximum age (1289–1177 cal BP, no. 30 in Table 1) and a limiting minimum age (1294–1126 cal BP, no. 29 in Table 1). This age is consistent with a radiocarbon age from a sample below the correlated event deposit of K-1 (1174–958 cal BP, no. 5 in Table 1) and two ages from samples above and below the correlated event deposit of K-2 (1290–1154 cal BP, no. 14 in Table 1; 1300–1177 cal BP, no. 15 in Table 1). The event deposits at K-3, K-6, and K-7 are common in their relative position below the light grayish inorganic mud layer (E8).

Event deposit E10 at K-4 is found at all locations but K-5. The depositional age of E10 at K-4 is constrained by two radiocarbon ages (1289–1177 cal BP, no. 30 in Table 1; 1404–1309 cal BP, no. 31 in Table 1). This age is consistent with radiocarbon ages below an event deposit at K-1 (1367–1294 cal BP, no. 6 in Table 1), above an event deposit at K-2 (1300–1177 cal BP, no. 15 in Table 1), and below an event deposit at K-3 (1404–1309 cal BP, no. 19 in Table 1). The event deposits observed at K-6 and K-7 were correlated with event deposit E10 at K-4 on the basis of their relative position to the white volcanic ash layer (E11).

Event deposit E11 of K-4, the volcanic ash layer with various sources, correlated with event layers found in K-2, K-3, K-6, and K-7. Because the event deposits were visible as white ash layers, preliminary correlation among cores was possible in the field. The event deposits consisting of volcanic ash at K-2, K-3, K-4, K-6, and K-7 were composed of glass shards. As shown by major chemical component analysis, the event deposits at K-3, K-4, K-6, and K-7 had in common that they contained glass erupted by different ages and different sources. The similar compositions of the volcanic glass shards within these event deposits and the radiocarbon ages from below and above the event deposits (1404–1309 cal BP, no. 19 in Table 1; 1404–1309 cal BP, no. 31 in Table 1; 1516–1353 cal BP, no. 32 in Table 1; and 1293–1177 cal BP, no. 45 in Table 1) enable correlation of the event layers among K-3, K-4, K-6, and K-7.

Event deposits E12, E13, and E14 of K-4 were found at K-1, K-2, K-6, and K-7. The three event deposits are present in organic mud dated between 1398–1308 cal BP (no. 33 in Table 1) and 1687–1414 cal BP (no. 34 in Table 1) at K-4, between 1367–1294 cal BP (no. 6 in Table 1) and 1829–1627 cal BP (no. 8 in Table 1) at K-1, older than 1293–1177 cal BP (no. 45 in Table 1) at K-6, and younger than 1821–1624 cal BP (no. 47 in Table 1) at K-7. These three event layers at K-2 were correlated by their depth in the cores and being stacks of three event layers.

E15 and E16 at K-4 are possibly correlated with two event deposits found at K-6. This correlation is based only on their stratigraphic positions (depth below the lake bottom).

4.2 Fossil diatom assemblages

We identified a total of 845 diatom taxa from 127 samples of core K-4 (Fig. 6 and Additional file 10: Table S5). The fossil diatom assemblages from Lake Kogare-ike were divided into freshwater plankton, freshwater–brackish plankton, freshwater tychoplankton, freshwater benthos, freshwater–brackish benthos, and brackish benthos based on their autecology (Fig. 6). Stratigraphically constrained cluster analysis was applied to identify 10 biostratigraphic zones (Zones 1–10 from top to bottom; Fig. 6). Detailed descriptions of each diatom zone are provided below.

The topmost zone 1 (0–29 cm depth) is characterized by a mixture of freshwater plankton (*Aulacoseira* spp. and *Discostella stelligera*) and freshwater–brackish plankton (*Cyclotella atomus*, *Cyclotella atomus* var. *gracilis*, and *Cyclotella meneghiniana*). Freshwater–brackish plankton (*C. atomus*, *C. atomus* var. *gracilis*, and *C. meneghiniana*) are dominant in organic mud samples of Zone 2 (29–79 cm depth). Assemblages within E1 belonging to Zone 2 contain the same dominant species of freshwater–brackish plankton as the assemblages in the organic mud of this zone. The brackish benthic diatom *Navicula gregaria* was also identified within E1. In Zones 3 (79–134.5 cm depth) and Zone 4 (134.5–163.5 cm depth), freshwater diatoms are dominant, except in the uppermost part of Zone 3 and within E3 of Zone 4. Zone 3 is characterized by freshwater tychoplankton (*Staurosira binodis*, *Staurosira construens*, and *Staurosira venter*) and freshwater benthos (*Gogorevia exilis*). Exceptionally, freshwater–brackish plankton (*C. atomus*, *C. atomus* var. *gracilis*, and *C. meneghiniana*) exhibits high relative abundance in the uppermost part of Zone 3. Zone 4 is dominated by the freshwater–brackish benthic species *Tabellaria fenestrata*, but assemblages within E3 are

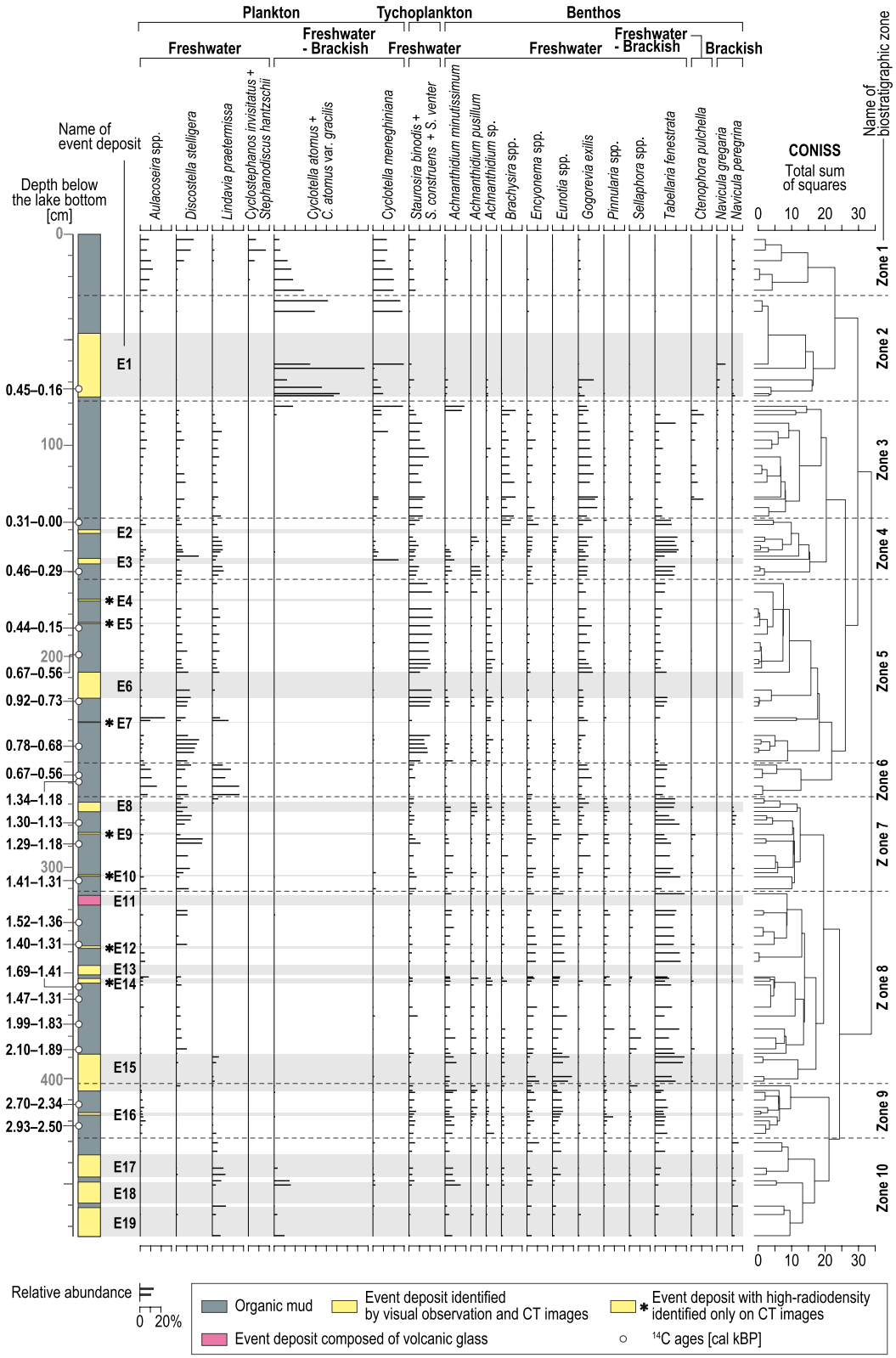

Fig. 6 Fossil diatom assemblages in the core from K-4. The term "relative abundance" denotes the percentage of the total diatom valves counted. The rightmost column shows the biostratigraphic zones based on stratigraphically constrained cluster analysis (Grimm 1987). Additional file 10: Table S5 shows the list of all diatom taxa and the count data

composed mainly of freshwater (*D. stelligera*) and freshwater–brackish (*C. meneghiniana*) plankton.

The assemblages in Zones 5–9 consist of freshwater species. In most assemblages classified in Zone 5 (163.5–250.5 cm depth), including the ones within E6, tychoplankton (*S. binodis*, *S. construens*, and *S. venter*) display high relative abundance. Zone 6 (250.5–266.5 cm depth) is dominated by freshwater plankton (*Aulacoseira* spp., *D. stelligera*, and *Lindavia praetermissa*). *Tabellaria fenestrata* and *G. exilis* are also recognized in this zone. Zone 7 (266.5–311.3 cm depth) is characterized by a mixture of the freshwater planktic species *D. stelligera* and the freshwater benthic species *T. fenestrata*. The assemblages within E8 are similar in composition to those in the organic mud samples of Zone 7. Assemblages within E9 and E10 were similar to those in the organic mud layer of zone 7 except for a slightly smaller relative abundance of *D. stelligera*. It should be noted that subsamples for E9, E10, and underlying and overlying layers were hard to be separated completely due to faint distributions of the event layers. Zone 8 (311.3–402.4 cm depth) and Zone 9 (402.4–428.3 cm depth) are dominated by freshwater benthos such as *Encyonema* spp., *Eunotia* spp., and *T. fenestrata*. The assemblages within E14 consist of the same taxa as those in Zone 8. In Zone 9, plankton exhibit a very low relative abundance. The division between Zone 8 and Zone 9 is identified within E15. Although both assemblages within E15 are dominated by freshwater benthos, the assemblages in Zone 8 contain a higher relative abundance of *T. fenestrata* and *Eunotia* spp. than those in Zone 9. This result is consistent with the character of the assemblages in the organic mud of each zone. The assemblages within E16 display a similar composition to those in the organic mud samples of Zone 9.

The assemblages in Zone 10 (428.3–475 cm depth) consist of a mixture of freshwater (*Lindavia praetermissa*) and freshwater–brackish (*C. meneghiniana*) plankton and freshwater benthos such as *Achnanthidium minutissimum*. The brackish benthic species *Navicula peregrina* is also present. The assemblages within E17–E19 have the same composition.

Diatom assemblages within the other 7 event deposits (E2, E4, E5, E7, and E11–E13) were not prepared for microscopic observation because it was not possible to sample those deposits separately from the inorganic mud above and below.

5 Discussion

5.1 Environmental history at the study site during the late Holocene

The fossil diatom assemblages reveal the paleoenvironmental changes recorded in Lake Kogare-ike sediments during the last 3000 years. A freshwater–brackish lagoonal environment is indicated by the freshwater and freshwater–brackish plankton in Zone 10 (Fig. 6). The decrease in these plankton and the increase in freshwater benthic taxa recognized at the boundary between Zones 10 and 9 show that the environment changed to a freshwater swamp/marsh that was isolated from the sea. The swampy environment lasted until 1300–1400 cal BP, the boundary between Zones 8 and 7. Plankton reappeared during deposition of the Zone 7 sediments, and the site consequently became a standing freshwater environment, as indicated by the dominance of freshwater plankton and tychoplankton in Zones 6–3. This environment continued until slightly before the deposition of E1.

The upward change in diatom assemblages from samples just below E1 to the top may represent eutrophication at this site. One of the most striking changes in diatom assemblages is the appearance of freshwater–brackish plankton (*C. atomus*, *C. atomus* var. *gracilis*, and *C. meneghiniana*). This appearance may simply reflect the increasing depth of the lake, but similar patterns have been reported in hypereutrophic conditions (Wolin and Duthie 1999; Wolin and Stone 2010). Nutrient increases caused by agricultural activity encourage phytoplankton growth, resulting in light limitation at the bottom of the lake. The light limitation disturbs growth of epipelic diatoms in the surface sediment and also macrophyte growth; these plants act as a substrate for epiphytic diatoms at the bottom of the lake. Consequently, the productivity of benthic (epiphytic and epipelic) diatoms at a eutrophic site sometimes approaches zero as plankton productivity and light limitation increase (Wolin and Duthie 1999; Wolin and Stone 2010). Agricultural activity around our study site can be recognized in the land use map for 1892, and aerial photographs from different times show that the paddy fields and farmland were abandoned around 2003 (Additional file 2: Fig. S1). The recent change in land use is consistent with the hypothesis of eutrophication due to human activity.

5.2 Age–depth model and depositional ages

A Bayesian age–depth model was constructed by using Bchron (Haslett and Parnell 2008; Parnell et al. 2008) based on the stratigraphy and radiocarbon ages and the peak of ^{137}Cs concentration from the core at K-4 (Fig. 7). The highest concentration of ^{137}Cs at 39.5 cm depth below the lake bottom corresponded to the global fallout peak in 1963 CE (Ritchie and McHenry 1990; Appleby 2001). The script is shown in Additional file 11: Text S1. The age–depth model provides the depositional ages of event deposits E1–E16 with 95% credible intervals (Fig. 7; Table 2; Additional file 12: Table S6). The deepest three event deposits E17–E19 were not applied to the model because we were unable to constrain their maximum

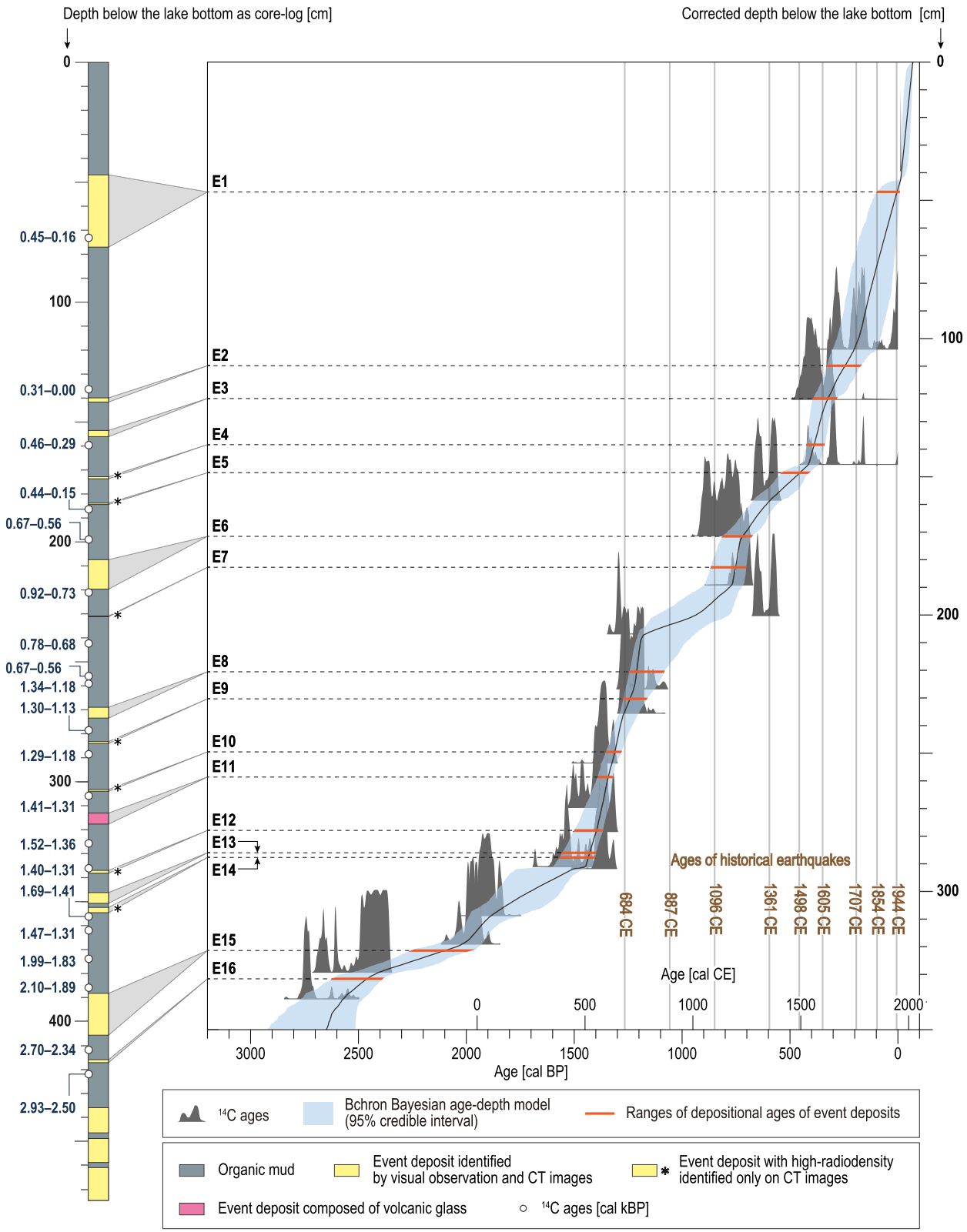

Fig. 7 Age–depth model reconstructed by using Bchron (Haslett and Parnell 2008; Parnell et al. 2008) for Bayesian chronological analysis. Event deposits were treated as instantaneous deposits, and their thicknesses were removed from the original core log of K-4. The scale on the *y*-axis shows the event-free depth. We constructed the model three times, and the averages of the three trials were used as the depositional ages. The results of each trial are provided in Additional file 12: Table S6

Table 2 Depositional ages of the event deposits (E1–E16) estimated by the Bayesian age-depth model

Core location	Name of event deposits	Corrected depth below the lake bottom (cm)	Calibrated depositional age (95% credible interval, cal BP)	Calibrated depositional age (95% credible interval, cal CE/BCE)
K-4	E1	46.9	100-present	1850–1960 CE
K-4	E2	109.8	330–164	1620–1786 CE
K-4	E3	121.7	394–277	1556–1673 CE
K-4	E4	138.4	430–338	1520–1612 CE
K-4	E5	148.5	535–412	1415–1538 CE
K-4	E6	171.5	818–675	1132–1275 CE
K-4	E7	182.7	871–704	1079–1246 CE
K-4	E8	220.5	1243–1070	707–880 CE
K-4	E9	230.3	1273–1154	677–796 CE
K-4	E10	249.5	1354–1279	596–671 CE
K-4	E11	258.6	1396–1320	554–630 CE
K-4	E12	277.9	1503–1367	447–583 CE
K-4	E13	286	1558–1399	392–551 CE
K-4	E14	287.7	1569–1404	381–546 CE
K-4	E15	321.4	2267–1976	317–26 BCE
K-4	E16	331.6	2615–2385	665–435 BCE

The model was consructed using Bchron (Haslett and Parnell 2008; Parnell et al. 2008). Event deposits were treated as instantaneous deposits, and their thickness were removed from the original core log of K-4. "Corrected depth below the lake bottom" represents the event-free depth

ages. We note that our model has uncertainties, in that it does not take erosion and redeposition prior to formation of event deposits into consideration.

The onset of ^{137}Cs also has the potential to constrain depositional ages, but was not applied to the age–depth model in this study for the following reasons. First, the onset of ^{137}Cs is regarded generally as corresponding to 1954 CE globally, when atmospheric nuclear weapons testing started (Pennington et al. 1973); however, in southwestern Japan, ^{137}Cs may have begun to accumulate in 1945 CE when the two atomic bombs were dropped on Hiroshima and Nagasaki (Saito-Kokubu et al. 2008). Second, the depth of the onset may be uncertain because cesium can migrate downward (e.g., Schimmack et al. 1997; Matisoff et al. 2011; Fujii et al. 2014), for example, via pore water (Takada et al. 2017).

5.3 Origin of event deposits

5.3.1 Tsunamis and storms

Event deposits formed by extreme waves are generally identified as relatively coarse sediment layers (sand and gravel) within fine deposits (mud and peat) in coastal lowlands (e.g., Atwater and Moore 1992; Donnelly and Woodruff 2007; Jankaew et al. 2008; Nelson et al. 2008; Dura et al. 2015). Tsunami geologists have extensively studied event deposits to differentiate tsunami from other event deposits, such as those formed by storms and flash flooding (e.g., Costa and Andrade 2020). Coarse deposits can be recognized as tsunami deposits by means of multiple sedimentological, paleontological, and geochemical techniques; for example, the sedimentary features of event deposits have been compared with features observed in recent tsunami deposits (e.g., the 2004 Indian Ocean tsunami: Moore et al. 2006 and Matsumoto et al. 2010; the 2011 Tohoku-oki tsunami: Goto et al. 2011 and Naruse et al. 2012). The presence of marine organisms and chemical indicators within event deposits has also been used to constrain the origin of those deposits (e.g., shells: Moore et al. 2006 and Donato et al. 2008; foraminifera: Nanayama and Shigeno 2006 and Pilarczyk et al. 2012, 2021; diatoms: Dawson 2007 and Sawai et al. 2009b, 2012; salt components: Szczuciński et al. 2005 and Chagué-Goff et al. 2012; biomarkers: Shinozaki et al. 2015 and Bellanova et al. 2020). We applied some of these types of evidence to infer the origin of the event deposits, as discussed below, although not all previously reported criteria are applicable to our data.

5.3.1.1 Sedimentological features of the event deposits Some sedimentological features are common in previously reported modern tsunami and storm deposits. Normal and inverse grading of grain size has been reported in both tsunami (e.g., Paris et al. 2007; Choowong et al. 2008a, b; Richmond et al. 2012; Matsumoto et al. 2023) and storm deposits (e.g., Wang and Horwitz 2007; Williams 2009). Rip-up clasts within event deposits are also common (e.g., Kortekaas and Dawson 2007; Goto et al. 2011; Putra et al. 2013), suggesting erosion of surface

sediments and its redeposition by high-velocity currents. In this study, changes in sand contents and the results of grain size analysis show that six event deposits at K-4 (E3, E6, E15, and E17–E19) exhibit either normal or inverse grading. Event deposit E8 includes rip-up clasts formed by light grayish inorganic mud at its base. Because the composition of the rip-up clasts (gray inorganic mud) is different from that of the contemporary lake bottom (brown organic mud), they may have been transported via muddy environments such as a channel and the bottom of the sea.

5.3.1.2 Spatial bias of the event deposits As has been demonstrated for recent tsunami and storm deposits on coastal lowlands, the spatial distributions of marine-originated event deposits are limited to seaward locations (Liu and Fearn 2000; Goff et al. 2004; Nakamura et al. 2012; Phantuwongraj and Choowong 2012; Pilarczyk et al. 2016) and the vicinity of inlets and barriers in coastal lakes (Matsumoto et al. 2010). This limitation is simply due to the decreased sediment transport capacity of tsunami or storm waves as they move away from the contemporary shoreline. At our study site, 13 of the 19 event deposits (E1–E10, E12–E14) occurred near the barrier (cores K-1, K-2, and K-3) and around the center of the lake (cores K-4, K-6, and K-7) (Figs. 2 and 3). The most inland core (K-5) included fewer event deposits than the other cores and contained event E1 and possibly E8 in samples younger than 1523–1383 cal BP (Fig. 2 and Table 1). The spatial distributions of the other events (E2–E7 and E9–E14) were not estimated, mainly because of the lack of cores between K-5 and the center of the lake, but they certainly did not have extensive distributions and were limited to around the center of the lake, which might suggest that the sediment was transported from the seaward direction.

5.3.1.3 Diatom assemblages Diatom assemblages within event deposits can be applied to infer the origin of the deposits because diatom species segregate according to their autecology and preferred substrate (Hemphill-Haley 1996; Dura and Hemphill-Haley 2020). The diatom assemblages within E1 contained higher relative abundances of brackish benthic species (*Navicula gregaria*) and freshwater–brackish planktonic taxa (*Cyclotella atomus*, *Cyclotella atomus* var. *gracilis*, and *C. meneghiniana*) than the muddy organic sediments below and above the event deposit. E3 also contained freshwater–brackish plankton (*C. meneghiniana*) within the event deposit, whereas samples below/above E3 were dominated by freshwater plankton (e.g., *Aulacoseira* spp., *Discostella stelligera*, and *Lindavia praetermissa*) and freshwater benthos (e.g., *Tabellaria fenestrata*). The diatom assemblages within E17–E19 consisted of freshwater, freshwater–brackish, and brackish species. These assemblages suggest that the sediments forming these three event deposits were transported by water from marine or brackish environments.

5.3.1.4 Simultaneity of event deposits and historical tsunamis and storms A common method to identify tsunami and storm deposits is to compare the constrained ages of the event deposits with those of known earthquakes and storms from documented history. When the depositional age of an event deposit corresponds to the age of a historical event, it has been accepted that the event deposit is a tsunami deposit associated with the earthquake or a storm deposit, such as in the following studies: the 1960 CE Chilean tsunami (Kempf et al. 2015); the 1964 CE Alaska tsunami (Shennan et al. 2014); the 1700 CE Cascadia tsunami (Atwater et al. 2005 as "The Orphan Tsunami of 1700"); and 13th-century typhoons in Kyushu (Woodruff et al. 2009).

The depositional ages of seven event deposits (E1–E5, E7, and E9) cover the range of historical records of tsunamis along the Nankai Trough. The depositional age of E1 (100 cal yr BP to the present; 1850–1960 CE) covers the 1944 Showa-Tonankai and the 1854 Ansei–Tokai tsunamis. The depositional age of E2 (330–164 cal BP; 1620–1786 CE) is consistent with the 1707 CE Hoei tsunami. The depositional ages of E3 (394–277 cal BP; 1556–1673 CE) and E4 (430–338 cal BP; 1520–1612 CE) cover the 1605 CE Keicho tsunami. The depositional ages of E5 (535–412 cal BP; 1415–1538 CE), E7 (871–704 cal BP; 1079–1246 CE), and E9 (1273–1154 cal BP; 677–796 CE) are consistent with the 1498 CE Meio, the 1096 CE Eicho (Kaho), and the 684 CE Hakuho earthquake, respectively.

The written record describes at least 55 storms that attacked areas around Ise Bay (Fig. 1d) between 1600 and 1865 CE (Arakawa et al. 1961; Additional file 1: Table S1). In addition, recent instrumental records show that 29 storms struck coastal areas of Mie Prefecture between 1945 and 2017 CE (Japan Meteorological Agency 2017). As for the earthquake history, the depositional ages of E1, E2, and E3 overlap the range of historical records of these numerous storms. Especially, the age of E1 (1850–1960 CE) covers the 1959 CE Isewan typhoon, which caused inundation and sea-level rise around Ise Bay including Minami-ise Town (Japan Meteorological Agency 1961; Editing Committee of the History of Nanto Town 1985).

5.3.1.5 Difference in frequency between storms and event deposit formation Storms occur at a much greater frequency than the event deposits around the study site. As mentioned above, the written record describes at least 55 storms between 1600 and 1865 CE (Arakawa et al. 1961) and 29 storms between 1945 and 2017 CE (Japan Meteorological Agency 2017). In contrast, the lacustrine sediments in this study record just 19 event deposits in the

last 3000 years. The frequency with which event deposits formed at the study site is thus much lower than the frequency of recorded storms. We therefore consider that the storms that frequently occur in the study area do not leave event deposits in the area every time, and that tsunamis and extraordinary storms are candidates for the causes of the event deposits. We could not estimate the precise intensity, inundation area, or damage of storms in historical records because of the fragmentary available information, but we are confident that the 1959 CE Isewan Typhoon is the most likely to be an extraordinary storm that had the potential to produce an event deposit on the lake floor at the study site.

Considering the discussion above, we attribute 13 event deposits (E1–E10 and E12–14) to marine inundation caused by tsunamis or extraordinary storms. Five of the 13 (E2, either E3 or E4, E5, E7, and E9), the ages of which are consistent with historical records of tsunamis, could be correlated with tsunamis associated with earthquakes along the Nankai Trough. The depositional age of E1 (100 cal yr BP to the present; 1850–1960 CE) covers the 1854 Ansei–Tokai tsunami, the 1944 CE Showa-Tonankai tsunami, and the 1959 CE Isewan typhoon. Our chronological data cannot distinguish these three events. We therefore conclude that E1 might be attributable to any of the three events, or to a combination of two or all three events. Furthermore, we are currently unable to definitively correlate event E8 with historical records. The 95% credible interval of the age of event E8 (1243–1070 cal yr BP; 707–880 CE) does not cover the 887 CE Ninna earthquake but is quite close. Considering analytical and statistical uncertainties of radiocarbon dating (Scott et al. 2007; Reimer et al. 2013), the possibility that E8 corresponds to the 887 CE event cannot be completely ruled out. For example, additional radiocarbon ages and subsequent reconstruction of the Bayesian age–depth model in future work may show an age overlap of E8 and the Ninna earthquake.

Either of E3 or E4 (one of which is not a tsunami deposit associated with the 1605 CE Keicho earthquake) and E6 are likely to have been deposited by extraordinary storm surges or unknown tsunamis. These event deposits are not correlated with any historical earthquakes, even though their depositional ages belong to the historical period. For E12–E14, it is unclear whether their origins are tsunamis or extraordinary storms because criteria (iii) (diatom assemblages) and (iv) (simultaneity of event deposits and historical tsunamis) cannot be applied.

5.3.2 Other causes

The volcanic ash layer (E11) probably resulted from erosion and reposition by a debris flow, a flash flood, or another temporary inflow. The distribution of E11 is limited to the central and landward parts of the lake (Figs. 2 and 3), implying that it was not formed by marine inundation. EDX analysis shows that E11 contains volcanic glass shards with different sources and eruption ages: glass shards from the Aira-Tn eruption (AT; 29–26 ka cal yr BP), the Kikai-Akahoya eruption (K-Ah; 7.3 ka cal BP), and the Amagi-Kawagodaira eruption (Kg; 3.1 ka cal yr BP), and shards similar in composition to those from eruptions in Niijima and Kozushima such as Iz-Kt (AD 838). This mixture of material indicates that E11 is not a single fallout volcanic ash, but resulted from redeposition. Therefore, we assume that older sediments surrounding Lake Kogare-ike (Fig. 1e) were eroded by intense rainfall and transported to our study site.

The origins of the five oldest event deposits (E15–E19) are also ambiguous in this study. These deposits were found only at K-4 and could not be laterally correlated because of the limited recovery of other cores. Because the diatom assemblages within E17–E19 contained freshwater–brackish plankton and slightly brackish benthos, these three may have been deposited by a marine-originated event, such as a tsunami or a storm. As indicated by the presence of freshwater–brackish and brackish diatom species in samples below and above E17–E19, the study site was more influenced by marine water during deposition of those units than at the present day, and might represent the process of change to a lagoonal environment.

5.4 Correlation with written documents and existing geological records

5.4.1 Historical earthquakes and tsunamis

The Bayesian age–depth model allows us to correlate the event deposits with historical tsunamis over the last 300 years that inundated our study site. Lake Kogare-ike records the 1707 Hoei tsunami (E2; 1620–1786 CE; Table 2) and either the 1944 Showa tsunami or the 1854 CE Ansei–Tokai, or a combination of both tsunamis (E1; 1850–1960 CE; Table 2). As mentioned above, we are not able to distinguish between 1944 and 1854 for the origin of the event layer. However, if E1 had been generated by only one of those events, our findings would indicate that the other tsunami did not leave a tsunami deposit on the lake bottom at our study site. Or, the geological record might have been erased as a result of bioturbation or anthropogenic disturbance, but we could not recognize clear evidence of either of these possibilities.

Either event deposit E3 (1556–1673 CE) or E4 (1520–1612 CE) may be new geological evidence for the 1605 CE Keicho earthquake. According to historical documents, a tsunami in 1605 affected Ise city, about 30 km northeast of our study site (Hatori 1975; Iida 1981). This tsunami damaged the entire coast along the Nankai

Trough (Hatori 1975; Iida 1981; Murakami et al. 1996), but its parent earthquake has remained uncertain. Some studies have concluded that the event was a tsunami earthquake (Yamamoto and Hagiwara 1995; Seno 2002), whereas others have suggested an earthquake off the southern part of the Kanto region (Tsuji 2016; Fig. 1d) or an earthquake in the Izu-Bonin trench (Ishibashi and Harada 2013; Fig. 1a). Further discussion of the rupture in 1605 requires detailed geological as well as historical research.

For historical tsunamis older than 1600 CE, the presence and absence of tsunami deposits at our study site are consistent with previously reported geological records in the Tonankai and Tokai regions, apart from the 887 CE Ninna tsunami. Event deposits E5 (1415–1538 CE; Table 2), E7 (1079–1246 CE), and E9 (677–796 CE) are consistent with the 1498 CE Meio tsunami, the 1096 CE Eicho tsunami, and the 684 Hakuho tsunami, respectively, and are correlated with tsunami deposits in the coastal lowlands at Shijima (Fujino et al. 2018; Fig. 1b) and Iwata (Fujiwara et al. 2020b; Fig. 1d). The absence of a 1361 tsunami deposit is also consistent with previous reports for the Tonankai and Tokai regions by Fujino et al. (2018) and Fujiwara et al. (2020b), respectively.

The predicted event age of E8 (707–880 CE) does not cover but is very close to the 887 Ninna earthquake. In previous work near our study site, an absence of tsunami deposits consistent with this earthquake was reported by Fujino et al. (2018) in the Shijima lowland (Fig. 1b), whereas liquefaction features and tsunami deposits probably correlated with the Ninna earthquake have been reported in the Tokai region (Sangawa 2013; Fujiwara et al. 2020a). Historical records of shaking and inundation associated with this earthquake have been mainly reported in Osaka and Kyoto (Fig. 1d), and damage in the Tokai and Tonankai segments is not definite (Ishibashi 1999, 2004).

5.4.2 Prehistoric earthquakes and tsunamis

Our prehistoric event deposits (E10 and E12–E16) are consistent with the geological records of tsunamis documented in previous studies. The depositional age of E10 (1354–1279 cal BP; Table 2) is consistent with the ages of tsunami deposits Sand C (1360–1080 cal yr BP; 590–870 CE) and Sand D (1400–1300 cal BP) in the Shijima lowland (Fujino et al. 2018; Fig. 1b). The age of Sand D also overlaps the age of our E12 (1503–1367 cal BP; Table 2). E12 (1503–1367 cal BP; Table 2), E13 (1558–1399 cal BP), and E14 (1569–1404 cal BP) can be correlated with the age of tsunami deposit OS-1 (1563–1454 cal BP, constrained event age recalibrated in this study with Oxcal 4.4 (Bronk Ramsey 2009) with the IntCal20 radiocarbon age calibration curve (Reimer et al. 2020) in the Osatsu lowland (Okahashi et al. 2005; Fig. 1b). The age of fourth most recent sand layer in Tsuji et al. (2002) was estimated by recalibration and modeling by Garrett et al. (2016) as 1520–1260 cal BP. This age overlaps the depositional ages of our E10 and E12–E14. The depositional ages of E15 (2267–1976 cal BP) and E16 (2615–2385 cal BP) overlap with those of a tsunami deposit (Sand F; 2660–2190 cal BP) in the Shijima lowland (Fujino et al. 2018) and with another tsunami deposit (2500–2000 cal BP) in coastal lake Sugari-oike, 30 km southwest of our study site (Okamura and Matsuoka 2012).

E15 is consistent with both tsunami deposits and with coastal uplift inferred from emergence of sessile assemblages at 2200 cal BP on the southern coast of the Kii Peninsula (Shishikura et al. 2008). We do not discuss correlations between E17–E19 and previous studies because their depositional ages are not constrained because of a lack of limiting maximum ages.

It should be noted that our age–depth model still has difficulty in statistically distinguishing the ages of adjacent events between E10 and E14. The 95% credible intervals of the ages of the events exhibit great overlap (Fig. 7), probably because too many extreme wave events (tsunamis and extraordinary storms) occurred during a short period of time relative to other intervals. More studies in adjacent areas and clearer correlations with those areas may lead to a better chronological reconstruction of marine inundations. We also note that the possibility that extraordinary storms are the origin of our prehistoric event deposits remains. At this stage, because of the large uncertainty of constrained event ages in both previous studies and this work, and the existence of only a few case studies, we could not establish definitive correlation of event deposits among sites or estimate whether each event represented extensive inundation.

6 Conclusions

Geological evidence for tsunami inundation along the Nankai Trough has been discussed during the last few decades; however, only a few studies have established well-constrained chronologies for deposits, and individual chronologies have covered only limited periods; for example, they lack records for the historical age because of anthropogenic modification. We obtained continuous sediment cores recording the period from 3000 years ago to the present and reconstructed the history of extreme waves by integrating X-ray CT observation and Bayesian age–depth modeling.

This study revealed the marine inundation history during the last 3000 years at Lake Kogare-ike, a coastal

lake in the Pacific coast of central Japan. Observation by the naked eye and X-ray CT images showed that the lacustrine sediments record 19 event deposits (E1–E19) interbedded with organic muddy sediments. Thirteen of the 19 event deposits (E1–E10 and E12–E14) were confirmed to occur near the barrier and around the central part of the lake in the study site. E1 and E8 were possibly recognized at all sampling locations. The diatom assemblages within E1 consisted of brackish and freshwater–brackish species, and those within E3 contained freshwater–brackish species. The frequency of inundation events in this study was much lower than the frequency of storms known from the historical records. On the basis mainly of changes in grain size, presence of rip-up clasts, distributions of event deposits, diatom assemblages, and information from historical records, we conclude that 13 of the 19 event deposits (E1–E10 and E12–E14) were formed by tsunamis or extraordinary storms. Bayesian age–depth models indicated that the five event deposits (E2, either of E3 or E4, E5, E7, and E9) are likely to be correlated with tsunami inundations associated with historical earthquakes along the Nankai Trough. E2 (1620–1786 CE), either of E3 (1556–1673 CE) or E4 (1520–1612 CE), E5 (1415–1538 CE), E7 (1079–1246 CE), and E9 (677–796 CE) are correlated with the 1707 CE Hoei, the 1605 CE Keicho, the 1498 CE Meio, the 1096 CE Eicho (Kaho), and the 684 CE Hakuho tsunamis, respectively. E1 (1850–1960 CE) may be a geological record of the 1944 CE Showa-Tonankai tsunami, the 1854 Ansei–Tokai tsunami, the 1959 Isewan typhoon, or a combination of two or all three events. There are no event deposits consistent with the 1361 CE Shohei tsunami at our study site. Despite such chronological correlation, it still remains possibility that some event deposits were formed by extraordinary storms. To solve this problem, it may be necessary to carry out inter-site (within a few tens of kilometers) and inter-regional (several tens of kilometers apart) correlations using a similar approach. Because storms generally affect only the specific area over which they pass, whereas a tsunami inundates the coastline along a distance of more than a hundred kilometers, storm and tsunami deposits may be distinguished by careful identification of event deposits and chronology. In this process, reexamination of event deposits and their chronology (including selection of appropriate materials and a Bayesian age–depth model) at other sites will contribute to significant progress in regional correlation and reconstructing rupture length for particular earthquake events, leading to reconstruction of the full history of coastal hazards along the Nankai Trough.

Abbreviations

BCE	Before common era
cal BP	Calibrated years before the present
CE	Common Era
CT	Computed tomography
T.P.	Tokyo Peil

Supplementary Information

The online version contains supplementary material available at https://doi.org/10.1186/s40645-023-00577-9.

Additional file 1: Table S1. A list of storms and flooding around Ise bay, reported in historical written documents.

Additional file 2: Figure S1. Aerial photographs and topographic maps showing topographic and land-use changes around Lake Kogare-ike. (a) Aerial photograph taken by the United States Army on 23 September 1947 (photograph number: USA-M500-75) (b) Aerial photograph taken by the Geospatial Information Authority of Japan on 16 May 1967 (photograph number: KK-676Y-C9-3). (c) Aerial photograph taken by the Geospatial Information Authority of Japan on 23 October 1980 (photograph number: KK-802X-C9-4). (d) Aerial photograph taken by the Geospatial Information Authority of Japan on 30 April 1990 (photograph number: KK-902X-C14-16). (e) Aerial photograph taken by the Geospatial Information Authority of Japan on 24 September 2008 (photograph number: CKK-2008-1X-C13A-13). (f) Topographic map at 1:20000 scale surveyed in 1892 and published in 1894 by the Land Survey Department of the Empire of Japan (map number: s988, map name: Ugura mura). (g) Topographic map at 1:50000 scale surveyed in 1892, modified in 1929, resurveyed in 1944, repaired in 1949, and published in 1952 by the Geographical Survey Institute (map number: 1997-7-4, map name: Nie ura). (h) Topographic map at 1:25000 scale surveyed in 1967 and published in 1969 by the Geospatial Information Authority of Japan (map number: 97-7-3-1, map name: Nie ura). (i) Topographic map at 1:25000 scale surveyed in 1967, modified based on an aerial photograph taken in 1980, correctively surveyed in 1982, and published in 1984 by the Geospatial Information Authority of Japan (map number: 97-7-3-3, map name: Nie ura). (j) Topographic map at 1:25000 scale surveyed in 1967, modified based on an aerial photograph taken in 1988, correctively surveyed in 1990, and published in 1991 by the Geospatial Information Authority of Japan (map number: 97-7-3-4B, map name: Nie ura).

Additional file 3: Figure S2. Photographs and X-ray CT images of the core sediments at K-4. The cores were mainly collected by using a Russian sampler. The uppermost sediments were obtained by push-core sampling.

Additional file 4: Figure S3. X-ray CT images of core sediments at K-1, K-2, K-3, K-5, K-6, and K-7. The cores were mainly collected by using a Russian sampler. The cores marked "*push-core" were obtained by push-core sampling.

Additional file 5: Figure S4. Photographs, X-ray CT images, and sketches of the event deposits identified at K-4 with the results of grain size analysis (sand content and grain size distribution of residual sand fractions).

Additional file 6: Table S2. Sedimentary features of event deposits (E1–E19).

Additional file 7: Table S3. Mud content, organic content, sand conent, and results of grain size analysis for redidual sand fractions.

Additional file 8: Figure S5. Scatter plots of MgO–SiO_2, CaO–SiO_2, Na_2O–SiO_2, and K_2O–SiO_2 of volcanic glass shards in event deposit E11 at sampling locations (a) K-3, (b) K-4, (c) K-6, and (d) K-7. Chemical compositions of the following tephras found in previous studies are also shown: AT and K-Ah (Machida and Arai 2003); Kg (Sugihara 1984); Iz-Kt and Nj-My (Sugihara 1984; Sugiuchi and Fukuoka 2005; Tsukui et al. 2006; Kobayashi et al. 2020; Murata et al. 2021); Kz-An, Kz-CbA and Kz-CbA' (Murata et al. 2021). Abbreviations: At, Aira-Tn tephra ; K-Ah, Kikai-Akahoya tephra; Kg, Amagi-Kawagodaira tephra; Iz-Kt, Kozushima-Tenjosan tephra; Nj-My, Niijima-Mukaiyama tephra; Kz-An, Kozushima-Ananoyama tephra;

Kz-CbA′, Kozushima-Chichibu-yama-A′ tephra; Kz-CbA, Kozushima-Chichibu-yama-A tephra.

Additional file 9: Table S4. Vertical change of ^{137}Cs concentrations at K-4.

Additional file 10: Table S5. Count data of fossil diatom analysis at K-4.

Additional file 11: Text S1. The R script for construction of an age–depth model using the "Bchron" library (Haslett and Parnell 2008; Parnell et al. 2008).

Additional file 12: Table S6. The depositional ages of event deposits (E1–E16) estimated in the three trials.

Acknowledgements
We acknowledge the landowners and the staff of the government office at Minami-ise town and the Ise-Shima National Park Management Office, Ministry of the Environment Government of Japan, who gave us permission to collect sediments at Lake Kogare-ike. We thank Andrew Parnell for his kind advice on constructing age–depth models with Bchron. The manuscript was improved by reviews from Philipp Kempf and two anonymous reviewers.

Author contributions
YSh and YSa proposed the topic and conceived and designed the study. YSh, YSa, DM, KT, YN, and MS collected sediment cores in the field. YN carried out a topographic survey. YSh picked out plant macrofossils for radiocarbon dating. YSa and YSh identified diatoms, and YSh counted diatoms. KI, YSh, and TT carried out the ^{137}Cs analysis. YSh wrote the initial manuscript, and YSa and TT produced the second version. YSh, YSa, DM, KT, KI, TT, YN, MS, and SF read and approved the final manuscript. A part of data in this study were taken as master's research of YSh. SF supervised YSh during the master's course.

Funding
This work was financially supported by the Geological Survey of Japan and the Ministry of Education, Culture, Sports and Technology of Japan. The latter is part of the Research Project for Compound Disaster Mitigation on the Great Earthquakes and Tsunamis around the Nankai Trough Region and the Research Project for Disaster Prevention on the great Earthquakes along the Nankai trough.

Availability of data and materials
All data integral to the stated conclusions are presented within the paper and Additional files (Figures S1–S5, Tables S1–S6, and Text S1).

Declarations

Competing interests
The authors declare that they have no competing interest.

Received: 18 August 2022 Accepted: 26 July 2023
Published online: 21 August 2023

References

Appleby PG (2001) Chronostratigraphic Techniques in Recent Sediments. In: Last WM, Smol JP (eds) Tracking Environmental Change Using Lake Sediments. Springer, Dordrecht

Arakawa H, Ishida Y, Ito T (1961) Nihon takashio shiryo. Meteorological Research Institute, Tokyo (**in Japanese**)

Atwater BF (1987) Evidence for great holocene earthquakes along the outer coast of Washington State. Science 236:942–944. https://doi.org/10.1126/science.236.4804.942

Atwater BF, Moore AL (1992) A tsunami about 1000 years ago in Puget Sound, Washington. Science 258:1614–1617. https://doi.org/10.1126/science.258.5088.1614

Atwater BF, Musumi-Rokkaku S, Satake K, Tsuji Y, Ueda K, Yamaguchi DK (2005) The orphan tsunami of 1700—Japanese clues to a parent earthquake in North America. U.S. Geological Survey Professional Paper 1707. University of Washington Press, Seattle

Baranes HE, Woodruff JD, Wallace DJ, Kanamaru K, Cook TL (2016) Sedimentological records of the C.E. 1707 Hōei Nankai Trough tsunami in the Bungo Channel, southwestern Japan. Nat Hazards 84:1185–1205. https://doi.org/10.1007/s11069-016-2498-3

Bellanova P, Frenken M, Reicherter K, Jaffe B, Szczuciński W, Schwarzbauer J (2020) Anthropogenic pollutants and biomarkers for the identification of 2011 Tohoku-oki tsunami deposits (Japan). Mar Geol 422:106117. https://doi.org/10.1016/j.margeo.2020.106117

Bianchette TA, Liu K, McCloskey TA (2022) A 4000-year paleoenvironmental reconstruction and extreme event record from Laguna Nuxco, Guerrero, Mexico. Palaeogeogr Palaeoclimatol Palaeoecol 594:110933. https://doi.org/10.1016/j.palaeo.2022.110933

Boespflug X, Long BFN, Occhietti S (1995) CAT-scan in marine stratigraphy: a quantitative approach. Mar Geol 122(4):281–301. https://doi.org/10.1016/0025-3227(94)00129-9

Bronk Ramsey C (2009) Bayesian analysis of radiocarbon dates. Radiocarbon 51(1):337–360. https://doi.org/10.1017/S0033822200033865

Central Meteorological Observatory (1945) Survey Overview of the December 7, Showa 19 Tonankai Earthquake. Central Meteorological Observatory, Tokyo (in Japanese)

Chagué-Goff C, Andrew A, Szczuciński W, Goff J, Nishimura Y (2012) Geochemical signatures up to the maximum inundation of the 2011 Tohoku-oki tsunami—implications for the 869 AD Jogan and other palaeotsunamis. Sediment Geol 282:65–77. https://doi.org/10.1016/j.sedgeo.2012.05.021

Choowong M, Murakoshi N, Hisada K, Charoentitirat T, Charusiri P, Phantuwongraj S, Wongkok P, Choowong A, Subsayjun R, Chutakositkanon V, Jankaew K, Kanjanapayont P (2008a) Flow conditions of the 2004 Indian Ocean tsunami in Thailand, inferred from capping bedforms and sedimentary structures. Terra Nova 20:141–149. https://doi.org/10.1111/j.1365-3121.2008.00799.x

Choowong M, Murakoshi N, Hisada K, Charusiri P, Charoentitirat T, Chutakositkanon V, Jankaew K, Kanjanapayont P, Phantuwongraj S (2008b) 2004 Indian Ocean tsunami inflow and outflow at Phuket, Thailand. Mar Geol 248:179–192. https://doi.org/10.1016/j.margeo.2007.10.011

Cisternas M, Atwater BF, Torrejón F, Sawai Y, Machuca G, Lagos M, Eipert A, Youlton C, Salgado I, Kamataki T, Shishikura M, Rajendran CP, Malik JK, Rizal Y, Husni M (2005) Predecessors of the giant 1960 Chile earthquake. Nature 437(7057):404–407. https://doi.org/10.1038/nature03943

Committees for Technical Investigation on Lessons Learned from Past Disasters (2008) The Report of the 1959 Isewan typhoon. Available via DIALOG. https://www.bousai.go.jp/kyoiku/kyokun/kyoukunnokeishou/rep/1959_isewan_typhoon/index.html of subordinate document. Accessed 11 Apr 2022 (in Japanese)

Costa PJM, Andrade C (2020) Tsunami deposits: present knowledge and future challenges. Sedimentology 67(3):1189–1206. https://doi.org/10.1111/sed.12724

Dawson S (2007) Diatom biostratigraphy of tsunami deposits: examples from the 1998 Papua New Guinea tsunami. Sediment Geol 200(3–4):328–335. https://doi.org/10.1016/j.sedgeo.2007.01.011

Dawson AG, Long D, Smith DE (1988) The Storegga Slides: evidence from eastern Scotland for a possible tsunami. Mar Geol 82(3–4):271–276. https://doi.org/10.1016/0025-3227(88)90146-6

Dawson AG, Dawson S, Bondevik S, Costa PJM, Hill J, Stewart I (2020) Reconciling Storegga tsunami sedimentation patterns with modelled wave heights: a discussion from the Shetland Isles field laboratory. Sedimentology 67(3):1344–1353. https://doi.org/10.1111/sed.12643

Donato SV, Reinhardt EG, Boyce JI, Rothaus R, Vosmer T (2008) Identifying tsunami deposits using bivalve shell taphonomy. Geology 36(3):199–202. https://doi.org/10.1130/G24554A.1

Donnelly JP, Woodruff JD (2007) Intense hurricane activity over the past 5,000 years controlled by El Niño and the West African monsoon. Nature 447:465–468

Dura T, Hemphill-Haley E (2020) Diatoms in tsunami deposits. In: Engel M, Pilarczyk J, May SM, Brill D, Garrett E (eds) Geological records of tsunamis and other extreme waves. Elsevier, Amsterdam

Dura T, Cisternas M, Horton BP, Ely LL, Nelson AR, Wesson RL, Pilarczyk JE (2015) Coastal evidence for Holocene subduction-zone earthquakes and tsunamis in central Chile. Quat Sci Rev 113:93–111. https://doi.org/10.1016/j.quascirev.2014.10.015

Editing Committee of the History of Nansei Town (2004) Nansei Choshi. Nansei Town, Mie (in Japanese)

Editing Committee of the History of Nanto Town (1985) Nanto Choshi. Nanto Town, Mie (in Japanese)

Education Center of Nanto Town (2000) Wasurenai! Anohi no o-tsunami. Tonankai jishin taiken kiroku. Nanto town, Mie (in Japanese)

Folk RL, Ward WC (1957) A study in the significance of grain-size parameters. J Sediment Res 27:3–26. https://doi.org/10.1306/74D70646-2B21-11D7-8648000102C1865D

Fujii K, Ikeda S, Akama A, Komatsu M, Takahashi M, Kaneko S (2014) Vertical migration of radiocesium and clay mineral composition in five forest soils contaminated by the Fukushima nuclear accident. Soil Sci Plant Nutr 60(6):751–764. https://doi.org/10.1080/00380768.2014.926781

Fujino S, Kimura H, Komatsubara J, Matsumoto D, Namegaya Y, Sawai Y, Shishikura M (2018) Stratigraphic evidence of historical and prehistoric tsunamis on the Pacific coast of Central Japan: implications for the variable recurrence of tsunamis in the Nankai trough. Quat Sci Rev 201:147–161. https://doi.org/10.1016/j.quascirev.2018.09.026

Fujiwara O, Goto K, Ando R, Garrett E (2020a) Paleotsunami research along the Nankai Trough and Ryukyu Trench subduction zones—current achievements and future challenges. Earth-Sci Rev 210:103333. https://doi.org/10.1016/j.earscirev.2020.103333

Fujiwara O, Aoshima A, Irizuki T, Ono E, Obrochta SP, Sampei Y, Sato Y, Takahashi A (2020b) Tsunami deposits refine great earthquake rupture extent and recurrence over the past 1300 years along the Nankai and Tokai fault segments of the Nankai Trough, Japan. Quat Sci Rev 227:105999. https://doi.org/10.1016/j.quascirev.2019.105999

Garrett E, Fujiwara O, Garrett P, Heyvaert VMA, Shihikura M, Yokoyama Y, Hubert-Ferrari A, Brückner H, Nakamura A, De Batist M, The QuakeRec-Nankai team (2016) A systematic review of geological evidence for Holocene earthquakes and tsunamis along the Nankai-Suruga Trough, Japan. Earth-Sci Rev 159:337–357. https://doi.org/10.1016/j.earscirev.2016.06.011

Godbout P, Roy M, Veillette JJ (2019) High-resolution varve sequences record one major late-glacial ice readvance and two drainage events in the eastern Lake Agassiz-Ojibway basin. Quat Sci Rev 223:105942. https://doi.org/10.1016/j.quascirev.2019.105942

Goff J, McFadgen BG, Chagué-Goff C (2004) Sedimentary differences between the 2002 Easter storm and the 15th-century Okoropunga tsunami, southeastern North Island. New Zealand Mar Geol 204(1–2):235–250. https://doi.org/10.1016/S0025-3227(03)00352-9

Goto K, Chagué-Goff C, Fujino S, Goff J, Jaffe B, Nishimura Y, Richmond B, Sugawara D, Szczuciński W, Tappin DR, Witter RC, Yulianto E (2011) New insights of tsunami hazard from the 2011 Tohoku-oki event. Mar Geol 290(1–4):46–50. https://doi.org/10.1016/j.margeo.2011.10.004

Grimm EC (1987) CONISS: a FORTRAN 77 program for stratigraphically constrained cluster analysis by the method of incremental sum of squares. Comput Geosci 13(1):13–35. https://doi.org/10.1016/0098-3004(87)90022-7

Haslett J, Parnell A (2008) A simple monotone process with application to radiocarbon-dated depth chronologies. J R Stat Soc C Appl Stat 57:399–418. https://doi.org/10.1111/j.1467-9876.2008.00623.x

Hatori T (1975) Sources of Large Tsunamis generated in the Boso, Tokai and Nankai Regions in 1498 and 1605. Bull Earthq Res Inst 50(2):171–185 (**in Japanese with English abstract**)

Hatori T (1978) Field Investigation of the Tokai Tsunamis in 1707 and 1854 along the Mie Coast, East Kii Peninsula. Bull Earthq Res Inst 53(1):1191–1225 (**in Japanese with English abstract**)

Hemphill-Haley E (1996) Diatoms as an aid in identifying late-Holocene tsunami deposits. The Holocene 6(4):439–448. https://doi.org/10.1177/095968369600600406

Hindson RA, Andrade C, Dawson AG (1996) Sedimentary processes associated with the tsunami generated by the 1755 Lisbon earthquake on the Algarve coast. Portugal Phys Chem Earth 21(1–2):57–63. https://doi.org/10.1016/S0079-1946(97)00010-4

Iida H (1981) Investigation of historical earthquakes (4): earthquake and tsunami damages by the Keicho Earthquake of February 3,1605. Bulletin of Aichi Institute of Technology 16:159–164 (**in Japanese with English abstract**)

Ishibashi K (1999) Great Tokai and Nankai, Japan, Earthquakes as Revealed by Historical Seismology. 1. Review of the Events until the mid-14th Century. J Geogr (Chigaku Zasshi) 108(4):399–423. https://doi.org/10.5026/jgeography.108.4_399. (**in Japanese with English abstract**)

Ishibashi K (2004) Status of historical seismology in Japan. Ann Geophys 47(2–3):339–368. https://doi.org/10.4401/ag-3305

Ishibashi K, Harada T (2013) Working Hypothesis of the 1605 Great Izu-Bonin Trench Earthquake and the 1614 Nankai Trough earthquake. In: Programme and Abstracts, the Seismological Society of Japan 2013 Fall Meeting, the Kanagawa Kenmin Hall and the Industry and the Trade Center, Kanagawa, 7–9 October 2013

Ishibashi K, Satake K (1998) Problems on forecasting great earthquakes in the subduction zones around Japan by means of Paleoseismology. Zisin (J Seismol Soc Jpn. 2nd ser.) 50(appendix):1–21. https://doi.org/10.4294/zisin1948.50.appendix_1

Ishibashi K (2014) Nankai Trough kyodai jishin: Rekishi, Kagaku, Syakai. Iwanami Shoten, Tokyo (in Japanese)

Ishimura D, Ishizawa T, Yamada M, Aoki K, Sato K (2022) Washover deposits related to tsunami and storm surge along the north coast of the Shimokita Peninsula in northern Japan. Prog Earth Planet Sci 9:69. https://doi.org/10.1186/s40645-022-00529-9

Jankaew K, Atwater B, Sawai Y, Choowong M, Charoentitirat T, Martin ME, Prendergast A (2008) Medieval forewarning of the 2004 Indian Ocean tsunami in Thailand. Nature 455:1228–1231

Japan Meteorological Agency (1961) Report of the Ise Bay Typhoon (No. 5915) in September 1959. Technical Report of the Japan Meteorological Agency 7:1–889 (in Japanese with English abstract)

Japan Meteorological Agency (2017) Major Meteorological Disasters in Mie Prefecture (since 1945). Available via DIALOG. https://www.jma-net.go.jp/tsu/knowledge/weather_disaster.pdf of subordinate document. Accessed 11 July 2022 (in Japanese)

Japan Meteorological Agency (2022a) Historical tide data Owase. Available via DIALOG. https://www.data.jma.go.jp/gmd/kaiyou/db/tide/sea_lev_var/sea_lev_var.php?stn=OW of subordinate document. Accessed 13 December 2022a (in Japanese)

Japan Meteorological Agency (2022b) Tidal observation data Owase. Available via DIALOG. https://www.data.jma.go.jp/gmd/kaiyou/db/tide/genbo/genbo.php?stn=OW of subordinate document. Accessed 13 December 2022b (in Japanese)

Juggins S (2022) Package 'rioja' https://cran.r-project.org/web/packages/rioja/rioja.pdf Accessed 4 March 2023

Kempf P, Moernaut J, Van Daele M, Vermassen F, Vandoorne W, Pino M, Urrutía R, Schmidt S, Garrett E, De Batist M (2015) The sedimentary record of the 1960 tsunami in two coastal lakes on Isla de Chiloé, south central Chile. Sediment Geol 328:73–86. https://doi.org/10.1016/j.sedgeo.2015.08.004

Kempf P, Moernaut J, Van Daele M, Vandoorne W, Pino M, Urrutia R, De Batist M (2017) Coastal lake sediments reveal 5500 years of tsunami history in south central Chile. Quat Sci Rev 161:99–116

Kempf P, Moernaut J, Van Daele M, Pino M, Urrutia R, De Batist M (2020) Paleotsunami record of the past 4300 years in the complex coastal lake system of Lake Cucao, Chiloé Island, south central Chile. Sediment Geol 401:105644

Kitamura A, Fujiwara O, Shinohara K, Akaike S, Masuda T, Ogura K, Urano Y, Kobayashi K, Tamaki C, Mori H (2013) Identifying possible tsunami deposits on the Shizuoka Plain, Japan and their correlation with earthquake activity over the past 4000 years. The Holocene 23(12):1684–1698. https://doi.org/10.1177/0959683613505345

Kobayashi M, Aoki K, Murata M, Nishizawa F, Suzuki T (2020) Tephrostratigraphy and Eruption History after Miyatsukayama Event on Niijima Volcano Izu Islands Japan. Bull Volcanol Soc Jpn 65(2):21–40. https://doi.org/10.18940/kazan.65.2_21. (**Japanese with English abstract**)

Kobayasi H, Idei M, Mayama S, Nagumo T, Osada K (2006) H. Kobayasi's atlas of Japanese diatoms based on electron microscopy 1. Uchida Rokakuho, Tokyo (in Japanese)

Komatsubara J, Okamura Y, Sawai Y, Shishikura M, Yoshimi M, Saomoto H (2007) Preliminary research of tsunami deposits along the coast of the Kii Peninsula. Ann Rep Active Fault Paleoearthq Res 7:219–230 (**in Japanese with English abstract**)

Kortekaas S, Dawson AG (2007) Distinguishing tsunami and storm deposits: an example from Martinhal. SW Portugal Sediment Geol 200(3–4):208–221. https://doi.org/10.1016/j.sedgeo.2007.01.004

Kosugi M (1988) Classification of living diatom assemblages as the indicator of environments, and its application to reconstruction of paleoenvironments. Quat Res (Daiyonki-Kenkyu) 27:1–20. https://doi.org/10.4116/jaqua.27.1. (**in Japanese with English abstract**)

Koyama M (1999) A review of historical seismology in Japan. J Geogr (chigaku Zasshi) 108(4):346–369. https://doi.org/10.5026/jgeography.108.4_346. (**in Japanese with English abstract**)

Krammer K, Lange-Bertalot H (1986) Süßwasserflora von Mitteleuropa. Bacillariophyceae 1. Teil: Naviculaceae. Gustav Fischer Verlag, Stuttgart

Krammer K, Lange-Bertalot H (1988) Süßwasserflora von Mitteleuropa. Bacillariophyceae 2. Teil: Bacillariaceae, Epithemiaceae, Surirellaceae. Gustav Fischer Verlag, Stuttgart

Krammer K, Lange-Bertalot H (1991a) Süßwasserflora von Mitteleuropa. Bacillariophyceae 3. Teil: Centrales, Fragilariaceae, Eunotiaceae. Gustav Fischer Verlag, Stuttgart

Krammer K, Lange-Bertalot H (1991b) Süßwasserflora von Mitteleuropa. Bacillariophyceae 4. Teil:Achnanthaceae Kritische Ergänzungen zu Navicula (Lineolatae) und Gomphonema. Gustav Fischer Verlag, Stuttgart

Liu K, Fearn ML (1993) Lake-sediment record of late Holocene hurricane activities from coastal Alabama. Geology 21(9):793–796. https://doi.org/10.1130/0091-7613(1993)021%3c0793:LSROLH%3e2.3.CO;2

Liu K, Fearn ML (2000) Reconstruction of prehistoric landfall frequencies of catastrophic hurricanes in northwestern Florida from lake sediment records. Quat Res 54(2):238–245. https://doi.org/10.1006/qres.2000.2166

Machida H, Arai F (2003) Atlas of tephra in and around Japan, revised. University of Tokyo Press, Tokyo

Matisoff G, Ketterer ME, Rosén K, Mietelski JW, Vitko LF, Persson H, Lokas E (2011) Downward migration of Chernobyl-derived radionuclides in soils in Poland and Sweden. Appl Geochemistry 26(1):105–115. https://doi.org/10.1016/j.apgeochem.2010.11.007

Matsumoto D, Shimamoto T, Hirose T, Gunatilake J, Wickramasooriya A, DeLile J, Young S, Rathnayake C, Ranasooriya J, Murayama M (2010) Thickness and grain-size distribution of the 2004 Indian Ocean tsunami deposits in Periya Kalapuwa Lagoon, eastern Sri Lanka. Sediment Geol 230(3–4):95–104. https://doi.org/10.1016/j.sedgeo.2010.06.021

Matsumoto D, Sawai Y, Tanigawa K, Namegaya Y, Shishikura M, Kagohara K, Fujiwara O, Shinozaki T (2023) Sedimentary diversity of the 2011 Tohoku-oki tsunami deposits on the Sendai coastal plain and the northern coast of Fukushima Prefecture. Japan Prog Earth Planet Sci 10:23. https://doi.org/10.1186/s40645-023-00553-3

Moore A, Nishimura Y, Gelfenbaum G, Kamataki T, Triyono R (2006) Sedimentary deposits of the 26 December 2004 tsunami on the northwest coast of Aceh, Indonesia. Earth Planets Space 58:253–258. https://doi.org/10.1186/BF03353385

Murakami H, Shimada T, Itoh S, Yamamoto N, Ishizuka J (1996) Reexamination of The Heights of The 1605, 1707 and 1854 Nankai Tsunamis along The Coast of Shikoku Island. J Jpn Soc Nat Disaster Sci 15(1):39–52 (**in Japanese with English abstract**)

Murata M, Kobayashi M, Aoki K, Takahashi T, Nishizawa F, Suzuki T (2021) Tephrostratigraphy and Eruption History of Kozushima Volcano, Izu Islands, Central Japan during the Last 30,000 Years. J Geogr (chigaku Zasshi) 130(3):379–402. https://doi.org/10.5026/jgeography.130.379(JapanesewithEnglishabstract)

Nagumo T (1995) Simple and safe cleaning methods for diatom samples. Diatom 10:88. https://doi.org/10.11464/diatom1985.10.0_88. (**in Japanese with English abstract**)

Nagumo T, Kobayasi H (1990) The Bleaching Method for gently loosening and cleaning a single diatom frustule. Diatom 5:45–50. https://doi.org/10.11464/diatom1985.5.0_45

Nakamura Y, Nishimura Y, Putra PS (2012) Local variation of inundation, sedimentary characteristics, and mineral assemblages of the 2011 Tohoku-oki tsunami on the Misawa coast, Aomori, Japan. Sediment Geol 282:216–227. https://doi.org/10.1016/j.sedgeo.2012.06.003

Namegaya Y, Tsuji Y (2005) Detailed distributions of Tsunami inundated heights in Mie Prefecture of the 1707 Hoei and the 1854 Ansei-Tokai Earthquake Tsunamis. Hist Earthq 20:33–56 (**in Japanese with English abstract**)

Nanayama F, Shigeno K (2006) Inflow and outflow facies from the 1993 tsunami in southwest Hokkaido. Sediment Geol 187(3–4):139–158. https://doi.org/10.1016/j.sedgeo.2005.12.024

Nanayama F, Satake K, Furukawa R, Shimokawa K, Atwater BF, Shigeno K, Yamaki S (2003) Unusually large earthquakes inferred from tsunami deposits along the Kuril trench. Nature 424:660–663

Naruse H, Arai K, Matsumoto D, Takahashi H, Yamashita S, Tanaka G, Murayama M (2012) Sedimentary features observed in the tsunami deposits at Rikuzentakata City. Sediment Geol 282:199–215. https://doi.org/10.1016/j.sedgeo.2012.08.012

Nelson AR, Sawai Y, Jennings AE, Bradley L, Gerson L, Sherrod BL, Sabean J, Horton BP (2008) Great-earthquake paleogeodesy and tsunamis of the past 2000 years at Alsea Bay, central Oregon coast, USA. Quat Sci Rev 27(7–8):747–768. https://doi.org/10.1016/j.quascirev.2008.01.001

Nishioka Y, Nakae S, Takeuchi K, Banno Y, Mizuno K, Ozaki M, Nakashima R, Sanematsu K, Nawa K, Komazawa M (2010) Geological map of Japan 1:200,000, Ise. Geological Survey of Japan, AIST, Tsukuba (in Japanese with English abstract)

Okada R, Umeda K, Kamataki T, Sawai Y, Matsumoto D, Shimada Y, Ioki K (2022) Geological record of 18th and 19th century tsunamis along the Japan Sea coast of Tsugaru Peninsula, northwestern Japan. Mar Geol 453:106. https://doi.org/10.1016/j.margeo.2022.106905

Okahashi H, Yasuhara M, Mitamura M, Hirose K, Yoshikawa S (2005) Event deposits associated with tsunamis and their sedimentary structure in Holocene marsh deposits on the east coast of the Shima Peninsula, central Japan. J Geosci Osaka City Univ 48:143–158

Okamura M, Matsuoka H (2012) Nankai earthquake recurrences from tsunami sediment. Kagaku 82(2):182–191 (**in Japanese**)

Paris R, Lavigne F, Wassmer P, Sartohadi J (2007) Coastal sedimentation associated with the December 26, 2004 tsunami in Lhok Nga, west Banda Aceh (Sumatra, Indonesia). Mar Geol 238:93–106. https://doi.org/10.1016/j.margeo.2006.12.009

Parnell AC, Haslett J, Allen JRM, Buch CE, Huntley B (2008) A flexible approach to assessing synchroneity of past events using Bayesian reconstructions of sedimentation history. Quat Sci Rev 27(19–20):1872–1885. https://doi.org/10.1016/j.quascirev.2008.07.009

Patrick R, Reimer C (1966) Diatoms of United States. Exclusive of Alaska and Hawaii. Volume 1. Academy of Natural Sciences of Philadelphia, Philadelphia

Patrick R, Reimer C (1975) Diatoms of United States Exclusive of Alaska and Hawaii, vol 2. Academy of Natural Sciences of Philadelphia, Philadelphia

Pennington W, Tutin TG, Cambray RS, Fisher EM (1973) Observations on Lake Sediments using Fallout ^{137}Cs as a Tracer. Nature 242:324–326. https://doi.org/10.1038/242324a0

Phantuwongraj S, Choowong M (2012) Tsunamis versus storm deposits from Thailand. Nat Hazards 63:31–50. https://doi.org/10.1007/s11069-011-9717-8

Pilarczyk JE, Horton BP, Witter RC, Vane CH, Chagué-Goff C, Goff J (2012) Sedimentary and foraminiferal evidence of the 2011 Tōhoku-oki tsunami on the Sendai coastal plain, Japan. Sediment Geol 282:78–89

Pilarczyk JE, Horton BP, Soria JLA, Switzer AD, Siringan F, Fritz HM, Khan NS, Ildefonso S, Doctor AA, Garcia ML (2016) Micropaleontology of the 2013 Typhoon Haiyan overwash sediments from the Leyte Gulf, Philippines. Sediment Geol 339:104–114. https://doi.org/10.1016/j.sedgeo.2016.04.001

Pilarczyk JE, Sawai Y, Namegaya Y, Tamura T, Tanigawa K, Matsumoto D, Shinozaki T, Fujiwara O, Shishikura M, Shimada Y, Dura T, Horton BP, Parnell AC, Vane CH (2021) A further source of Tokyo earthquakes and Pacific Ocean tsunamis. Nat Geosci 14:796–800. https://doi.org/10.1038/s41561-021-00812-2

Putra PS, Nishimura Y, Nakamura Y, Yulianto E (2013) Sources and transportation modes of the 2011 Tohoku-Oki tsunami deposits on the central east Japan coast. Sediment Geol 294:282–293. https://doi.org/10.1016/j.sedgeo.2013.06.004

R Core Team (2021) R: a language and environment for statistical computing. https://www.R-project.org/ Accessed 7 Apr 2022

Reimer PJ, Bard E, Bayliss A, Beck JW, Blackwell PG, Bronk Ramsey C, Brown DM, Buck CE, Edwards RL, Friedrich M, Grootes PM, Guilderson TP, Haflidason H, Hajdas I, Hatté C, Heaton TJ, Hogg AG, Hughen KA, Kaiser KF, Kromer B, Manning SW, Reimer RW, Richards DA, Scott EM, Southon JR, Turney CSM, van der Plicht J (2013) Selection and treatment of data

for radiocarbon calibration: an update to the international calibration (IntCal) Criteria. Radiocarbon 55(4):1923–1945. https://doi.org/10.2458/azu_js_rc.55.16955

Reimer PJ, Austin WEN, Bard E, Bayliss A, Blackwell PG, Bronk Ramsey C, Butzin M, Cheng H, Edwards RL, Friedrich M, Grootes PM, Guilderson TP, Hajdas I, Heaton TJ, Hogg AG, Hughen KA, Kromer B, Manning SW, Muscheler R, Palmer JG, Pearson C, van der Plicht J, Reimer RW, Richards DA, Scott EM, Southon JR, Turney CSM, Wacker L, Adolphi F, Büntgen U et al (2020) The IntCal20 Northern hemisphere radiocarbon age calibration curve (0–55 cal kBP). Radiocarbon 62(4):725–757. https://doi.org/10.1017/RDC.2020.41

Richmond B, Szczuciński W, Chagué-Goff C, Goto K, Sugawara D, Witter R, Tappin DR, Jaffe B, Fujino S, Nishimura Y, Goff J (2012) Erosion, deposition and landscape change on the Sendai coastal plain, Japan, resulting from the March 11, 2011 Tohoku-oki tsunami. Sediment Geol 282:27–39. https://doi.org/10.1016/j.sedgeo.2012.08.005

Ritchie JC, McHenry JR (1990) Application of radioactive fallout cesium-137 for measuring soil Erosion and sediment accumulation rates and patterns: a review. J Environ Qual 19(2):215–233. https://doi.org/10.2134/jeq1990.00472425001900020006x

Sabatier S, Wilhelm B, Ficetola GF, Moiroux F, Poulenard J, Develle A, Bichet A, Chen W, Pignol C, Reyss J, Gielly L, Bajard M, Perrette Y, Malet E, Taberlet P, Arnaud F (2017) 6-kyr record of flood frequency and intensity in the western Mediterranean Alps—Interplay of solar and temperature forcing. Quat Sci Rev 170:121–135. https://doi.org/10.1016/j.quascirev.2017.06.019

Saito-Kokubu YK, Magara M, Miyamoto Y, Sakurai S, Usuda S, Yamazaki H, Yoshikawa S, Nagaoka S, Mitamura M, Inoue J, Murakami A (2008) Depositional records of plutonium and ^{137}Cs released from Nagasaki atomic bomb in sediment of Nishiyama reservoir at Nagasaki. J Environ Radioact 99(1):211–217. https://doi.org/10.1016/j.jenvrad.2007.11.010

Sangawa A (2013) The paper for the 2011 Japan Association for Quaternary Research Academic Award. Research results of earthquake-archaeology. Quat Res (Daiyonki-Kenkyu) 52(5):191–202. https://doi.org/10.4116/jaqua.52.191. (**in Japanese with English abstract**)

Sangawa A (2007) Jishin no nihonshi (earthquakes in Japanese history). Chuokoron-shinsha, Tokyo (in Japanese)

Satake K, Atwater BF (2007) Long-term perspectives on giant earthquakes and tsunamis at subduction zones. Annu Rev Earth Planet Sci 35:349–374. https://doi.org/10.1146/annurev.earth.35.031306.140302

Sawai Y (2020) Subduction zone paleoseismology along the Pacific coast of northeast Japan—progress and remaining problems. Earth Sci Rev 208:103261. https://doi.org/10.1016/j.earscirev.2020.103261

Sawai Y, Jankaew K, Martin ME, Prendergast A, Choowong M, Charoentitirat T (2009a) Diatom assemblages in tsunami deposits associated with the 2004 Indian Ocean tsunami at Phra Thong Island, Thailand. Mar Micropaleontol 73:70–79. https://doi.org/10.1016/j.marmicro.2009.07.003

Sawai Y, Kamataki T, Shishikura M, Nasu H, Okamura Y, Satake K, Thomson KH, Matsumoto D, Fujii Y, Komatsubara J, Aung TT (2009b) Aperiodic recurrence of geologically recorded tsunamis during the past 5500 years in eastern Hokkaido, Japan. J Geophys Res 114:B01319. https://doi.org/10.1029/2007JB005503

Sawai Y, Namegaya Y, Okamura Y, Satake K, Shishikura M (2012) Challenges of anticipating the 2011 Tohoku earthquake and tsunami using coastal geology. Geophys Res Lett 39:L21309. https://doi.org/10.1029/2012GL053692

Schimmack W, Flessa H, Bunzl K (1997) Vertical migration of Chernobyl-derived radiocesium in Bavarian grassland soils. Naturwissenschaften 84:204–207. https://doi.org/10.1007/s001140050379

Scott EM, Cook GT, Naysmith P (2007) Error and uncertainty in radiocarbon measurements. Radiocarbon 49(2):427–440. https://doi.org/10.1017/S0033822200042351

Seno T (2002) Tsunami earthquakes as transient phenomena. Geophys Res Lett 29(10):581–584. https://doi.org/10.1029/2002GL014868

Shennan I, Bruhn R, Barlow N, Good K, Hocking E (2014) Late Holocene great earthquakes in the eastern part of the Aleutian megathrust. Quat Sci Rev 84:86–97. https://doi.org/10.1016/j.quascirev.2013.11.010

Shimada Y, Fujino S, Sawai Y, Tanigawa K, Matsumoto D, Momohara A, Saito-Kato M, Yamada M, Hirayama E, Suzuki T, Chagué C (2019) Geological record of prehistoric tsunamis in Mugi town, facing the Nankai Trough, western Japan. Prog Earth Planet Sci 6:33. https://doi.org/10.1186/s40645-019-0279-9

Shinozaki T, Fujino S, Ikehara M, Sawai Y, Tamura T, Goto K, Sugawara D, Abe T (2015) Marine biomarkers deposited on coastal land by the 2011 Tohoku-oki tsunami. Nat Hazards 77:445–460. https://doi.org/10.1007/s11069-015-1598-9

Shishikura M, Echigo T, Maemoku H, Ishiyama T (2008) Height and ages of uplifted sessile assemblage distributed along the southern coast of the Kii Peninsula, south-central Japan - Reconstruction of multi-segment earthquake history along the Nankai Trough. Ann Report Active Fault Paleoearthq Res 8:267–280 (**in Japanese with English abstract**)

Simonsen R (1987) Atlas and catalogue of the diatom types of friedrich Hustedt. J. Cramer Verlag, Stuttgart

Sugawara D, Minoura K, Imamura F (2008) Tsunamis and tsunami sedimentology. In: Shiki T, Tsuji Y, Yamazaki T, Minoura K (eds) Tsunamiites. Elsevier, Amsterdam

Sugihara S (1984) Mineral description characteristics and eruptive ages of time-marker tephra in Naga Trench of Tanna fault. Chikyu Mon 6:171–177 (**in Japanese**)

Sugiuchi Y, Fukuoka T (2005) Distinction between Kozushima Tenjo-san AD838 Tephra and Niijima Mukai-yama AD886 Tephra by chemical composition based on EPMA –For highly accurate Fuji volcano eruption history during AD800–1000–. PROGRAMME and ABSTRACTS. Jpn Assoc Quat Res 35:133–134 (**in Japanese**)

Szczuciński W (2012) The post-depositional changes of the onshore 2004 tsunami deposits on the Andaman Sea coast of Thailand. Nat Hazards 60:115–133. https://doi.org/10.1007/s11069-011-9956-8

Szczuciński W, Niedzielski P, Rachlewicz G, Sobczyński T, Zioła A, Kowalski A, Lorenc S, Siepak J (2005) Contamination of tsunami sediments in a coastal zone inundated by the 26 December 2004 tsunami in Thailand. Environ Geol 49:321–331. https://doi.org/10.1007/s00254-005-0094-z

Takada M, Yamada T, Takahara T, Endo S, Tanaka K, Kajimoto T, Okuda T (2017) Temporal changes in vertical distribution of ^{137}Cs in litter and soils in mixed deciduous forests in Fukushima. Japan J Nucl Sci Technol 54(4):452–458. https://doi.org/10.1080/00223131.2017.1287602

Tanigawa K, Shishikura M, Fujiwara O, Namegaya Y, Matsumoto D (2018) Mid- to late-Holocene marine inundations inferred from coastal deposits facing the Nankai Trough in Nankoku, Kochi Prefecture, southern Japan. The Holocene 28(6):867–878. https://doi.org/10.1177/0959683617752837

The Headquarters for Earthquake Research Promotion (2013) Evaluations of occurrence potentials of subduction-zone earthquakes. Available via DIALOG. https://www.jishin.go.jp/main/chousa/kaikou_pdf/nankai_2.pdf of subordinate document. Accessed 7 March 2022 (in Japanese)

Tsuji Y, Okamura M, Matsuoka H, Goto T, Han SS (2002) Prehistorical and historical tsunami traces in lake floor deposits, Oike Lake, Owase City and Suwaike Lake, Kii-Nagashima City, Mie Prefecture, central Japan. Chikyu Mon 24:743–747 (**in Japanese**)

Tsuji Y (2016) Height Distribution of the Tsunami of the South Kanto Earthquake of February 3rd, 1605. Abstract H-DS19 presented at the Japan Geoscience Union Meeting 2016, Makuhari, Japan, 22–26 May 2016. https://confit.atlas.jp/guide/event/jpgu2016/subject/HDS19-18/detail Accessed 20 July 2022

Tsukui M, Koichiro Saito K, Hayashi K (2006) Frequent and Intensive Eruptions in the 9th Century, Izu Islands, Japan: Revision of Volcano-Stratigraphy Based on Tephras and Historical Document. Bull Volcanol Soc Jpn 51(5):327–338. https://doi.org/10.18940/kazan.51.5_327. (**in Japanese with English abstract**)

Usami T, Ishii H, Imamura T, Takemura M, Matsumura R (2013) Materials for comprehensive list of destructive earthquakes in Japan, 599–2012. University of Tokyo Press, Tokyo (in Japanese)

Wang P, Horwitz MH (2007) Erosional and depositional characteristics of regional overwash deposits caused by multiple hurricanes. Sedimentology 54:545–564. https://doi.org/10.1111/j.1365-3091.2006.00848.x

Watanabe H (1998) Comprehensive list of tsunamis to hit the Japanese islands [second edition]. University of Tokyo Press, Tokyo (in Japanese)

Wessel P, Smith WHF, Scharroo R, Luis J, Wobbe F (2013) Generic Mapping Tools: improved version released. EOS Trans AGU 94(45):409–410. https://doi.org/10.1002/2013EO450001

Williams HFL (2009) Stratigraphy, sedimentology, and microfossil content of hurricane rita storm surge deposits in Southwest Louisiana. J Coast Res 25(4):1041–1051. https://doi.org/10.2112/08-1038.1

Wolin JA, Duthie HC (1999) Diatoms as indicators of water level change in freshwater lakes. In: Stoermer EF, Smol JP (eds) The diatoms: applications for the environmental and earth sciences. Cambridge University Press, Cambridge

Wolin JA, Stone JR (2010) Diatoms as indicators of water-level change in freshwater lakes. In: Smol JP, Stoermer EF (eds) The diatoms: applications for the environmental and earth sciences, 2nd edn. Cambridge University Press, Cambridge

Woodruff JD, Donnelly JP, Okusu A (2009) Exploring typhoon variability over the mid-to-late Holocene: evidence of extreme coastal flooding from Kamikoshiki, Japan. Quat Sci Rev 28(17–18):1774–1785. https://doi.org/10.1016/j.quascirev.2009.02.005

Yamada K, Omori T, Kitaba I, Hori H, Nakagawa T (2021) Extraction method for fossil pollen grains using a cell sorter suitable for routine 14C dating. Quat Sci Rev 272:107236. https://doi.org/10.1016/j.quascirev.2021.107236

Yamamoto T, Hagiwara T (1995) On the earthquake of 16 December Keicho era (1605): a tsunami earthquake off Tokai and Nankai? In: Hagiwara T (ed) Search for Paleo-earthquakes: approach to offshore earthquakes. University of Tokyo Press, Tokyo (**in Japanese**)

Yao Q, Liu K, Rodrigues E, Bianchette T, Aragón-Moreno AA, Zhang Z (2020) A geochemical record of Late-Holocene hurricane events from the Florida Everglades. Water Resour Res 56(8):e2019WR026857. https://doi.org/10.1029/2019WR026857

Publisher's Note